# nature communications



**Article** 

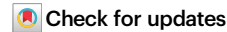
https://doi.org/10.1038/s41467-025-59278-0

# Injectable extracellular vesicle hydrogels with tunable viscoelasticity for depot vaccine

Received: 31 March 2024

Accepted: 16 April 2025

Published online: 22 April 2025



Rimsha Bhatta<sup>1</sup>, Joonsu Han 📵 <sup>1</sup>, Yusheng Liu<sup>1</sup>, Yang Bo 📵 <sup>1</sup>, Yueji Wang<sup>1</sup>, Daniel Nguyen<sup>1</sup>, Qian Chen 📵 <sup>1,2,3</sup> & Hua Wang 📵 <sup>1,2,3,4,5,6,7</sup> ⋈

Extracellular vesicles (EVs) have been actively explored for therapeutic applications in the context of cancer and other diseases. However, the poor tissue retention of EVs has limited the development of EV-based therapies. Here we report a facile approach to fabricating injectable EV hydrogels with tunable viscoelasticity and gelation temperature, by metabolically tagging EVs with azido groups and further crosslinking them with dibenzocyclooctyne-bearing polyethylene glycol via efficient click chemistry. One such EV gel has a gelation temperature of 39.4 °C, enabling in situ gelation of solution-form EVs upon injection into the body. The in situ formed gels are stable for over 4 weeks and can attract immune cells including dendritic cells over time in vivo. We further show that tumor EV hydrogels, upon subcutaneous injection, can serve as a long-term depot for EV-encased tumor antigens, providing an extended time for the modulation of dendritic cells and subsequent priming of tumor-specific CD8<sup>+</sup> T cells. The tumor EV hydrogel also shows synergy with anti-PD-1 checkpoint blockade for tumor treatment, and is able to reprogram the tumor microenvironment. As a proof-of-concept, we also demonstrate that EV hydrogels can induce enhanced antibody responses than solution-form EVs over an extended time. Our study yields a facile and universal approach to fabricating injectable EV hydrogels with tunable mechanics and improving the therapeutic efficacy of EV-based therapies.

Extracellular vesicles (EVs) are nanosized vesicles secreted by nearly all types of cells and inherit a variety of molecules including lipids, proteins, RNAs, and other metabolites from the parent cells<sup>1–5</sup>. Hence, they play a critical role in cellular communication and have raised widespread interest in exploring their diagnostic and therapeutic applications<sup>6–8</sup>. Diagnostically, EVs have been actively explored as the blood biomarker for various types of cancers, based on the hypothesis that cancer-secreted EVs can reach the blood circulation<sup>9–11</sup>. Therapeutically, EVs can transfer bioactive molecules from the parent cells to the recipient cells, and thus modulate the function of recipient cells

and tune the intercellular interactions. For example, EVs derived from mesenchymal stem cells (MSCs) are actively explored as therapeutics for tissue injuries including spinal cord injury<sup>12</sup>, myocardial infarction<sup>13,14</sup> and muscle injury<sup>15–20</sup>, with over 40 MSC EV-based therapies under clinical trials<sup>21–23</sup>. Starting from early 1980s, tumor-secreted EVs have also been actively explored for the development of cancer vaccines<sup>24–30</sup>. Tumor EVs contain tumor-associated antigens that can be processed and presented by antigen presenting cells in the body<sup>31–33</sup>, for subsequent elicitation of tumor-specific T cell response<sup>34–36</sup>. While tumor EVs may inherit virulence factors or toxic

<sup>1</sup>Department of Materials Science and Engineering, University of Illinois at Urbana-Champaign, Urbana, IL, USA. <sup>2</sup>Beckman Institute for Advanced Science and Technology, University of Illinois at Urbana-Champaign, Urbana, IL, USA. <sup>3</sup>Materials Research Laboratory, University of Illinois at Urbana-Champaign, Urbana, IL, USA. <sup>4</sup>Cancer Center at Illinois (CCIL), Urbana, IL, USA. <sup>5</sup>Department of Bioengineering, University of Illinois at Urbana-Champaign, Urbana, IL, USA. <sup>6</sup>Carle College of Medicine, University of Illinois at Urbana-Champaign, Urbana, IL, USA. <sup>7</sup>Institute for Genomic Biology, University of Illinois at Urbana-Champaign, Urbana, IL, USA. <sup>8</sup>Cancer Center at Illinois at Urbana-Champaign, Urbana, IL, USA. <sup>8</sup>Cancer Center at Illinois (CCIL), Urbana, IL, USA. <sup>8</sup>Cancer Center at Il

metabolites from parent tumor cells, various clinical trials have demonstrated their benign safety profiles as a promising candidate for therapeutic cancer vaccines<sup>37–44</sup>. However, existing tumor EV vaccines are limited by the modest efficacy, partially due to the limited amount of tumor antigens and insufficient activation of antigen presenting cells in the body<sup>45</sup>. In current practice, EVs are often administered in a solution form into the tissue of interest or systemically into the bloodstream<sup>46–48</sup>. The poor tissue retention of EVs, despite the administration of a high number of EVs or multiple doses, often dampens the overall efficacy. To enhance the tissue retention of EVs, efforts were made to encapsulate EVs in a hydrogel or scaffold<sup>49–52</sup>, which however is limited by the low EV loading efficiency and the lack of control over the exposure of EVs to cells of interest.

Here we show that EV itself can serve as the main building block of hydrogels, by metabolically tagging EVs and then crosslinking them into a

gel network via efficient click chemistry. We previously demonstrated that metabolic glycan labeling of cells provides a facile approach to generating chemically tagged EVs<sup>53</sup>. Once internalized by cells, unnatural sugars bearing clickable chemical tags (e.g., tetraacetyl *N*-azidoacetylmannosamine (Ac<sub>4</sub>ManNAz)) can undergo the metabolic glycoengineering processes, conjugate to proteins and lipids, and become expressed on the cell membrane in the form of glycoproteins and glycolipids<sup>46-60</sup>. Since EVs inherit a portion of the cell membrane, EVs secreted by the labeled cells also carry the chemical tags (e.g., azido group)<sup>53</sup>. These azido-tagged EVs can react with dibenzocyclooctyne (DBCO)-functionalized 8-arm polyethylene glycol (PEG) via efficient click chemistry<sup>61-63</sup> to yield a fully crosslinked gel network (Fig. 1a). The gelation temperature, stiffness, viscoelasticity, as well as the injectability of the fabricated EV gels can be tuned by adjusting the concentration of EVs. At certain concentrations, the mixture of azido-tagged EVs and DBCO-

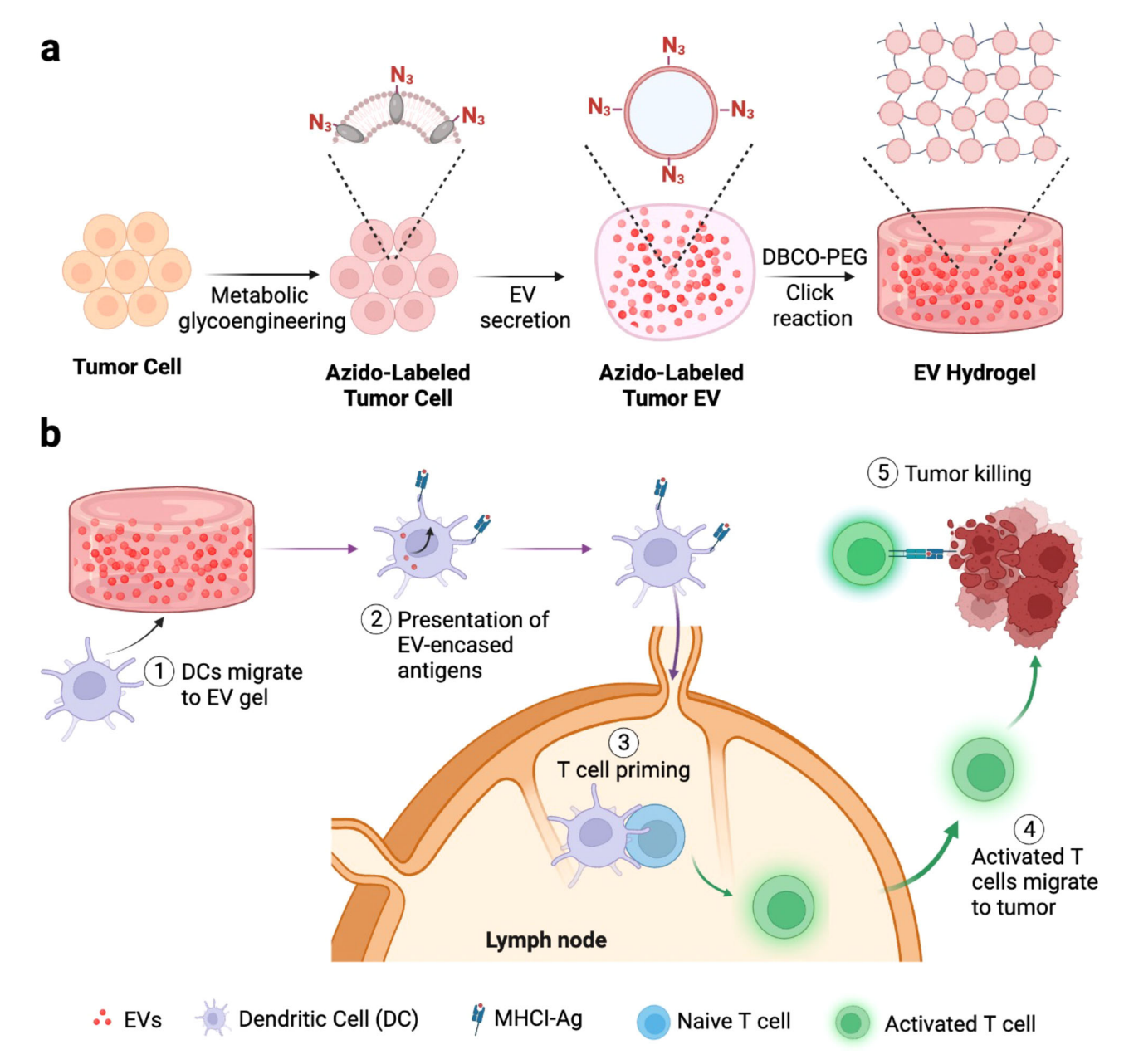


**Fig. 1** | **Injectable EV hydrogels for depot vaccines. a** Schematic illustration of metabolic tagging of extracellular vesicles (EVs) and subsequent formation of EV hydrogels via click chemistry. **b** EV hydrogels for therapeutic cancer vaccines. Injectable EV hydrogels can persist for weeks in vivo, allowing for sustained

modulation of dendritic cells (DCs) that can process and present EV-encased tumor antigens. Tumor antigen-presenting DCs can then migrate to lymph nodes to prime tumor-specific CD8<sup>+</sup>T cells for eventual tumor killing. Figures **a** and **b** were created using Biorender.

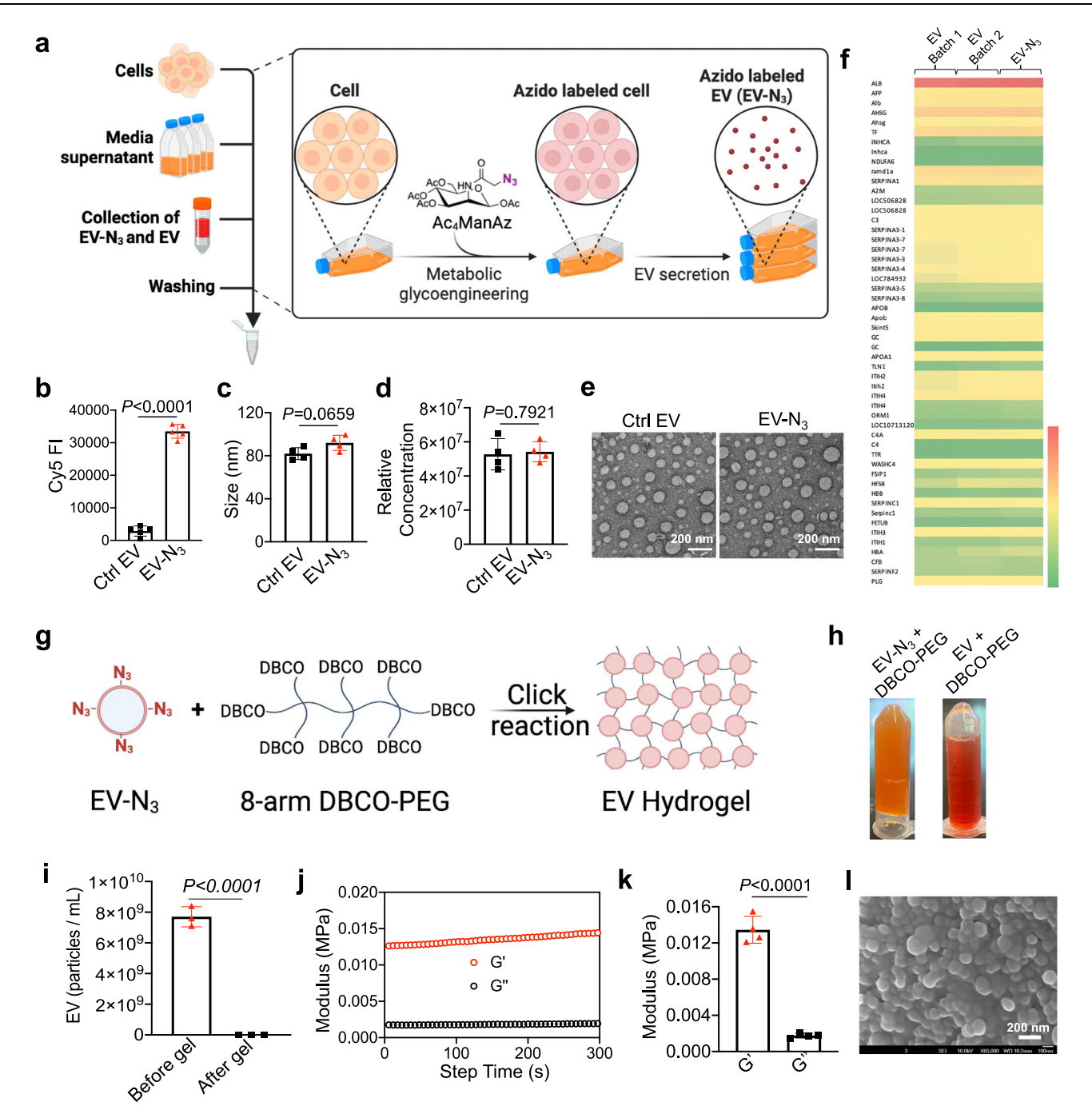


**Fig. 2** | **Synthesis and characterization of EV hydrogels. a** Schematic illustration of labeling of cancer cells with azido group and subsequent secretion of azido-labeled EVs (created using Biorender). **b** Cy5 fluorescence intensity of E.G7-OVA EVs that were incubated with DBCO-Cy5 for 30 min (n = 5 technical replicates). Also shown are the **c** average diameter (n = 4 technical replicates), **d** relative concentration (n = 4 technical replicates), and **e** TEM images of azido-labeled EVs and control EVs derived from E.G7-OVA cells. **f** Proteomic analysis of azido-labeled and control E.G7-OVA EVs. Two different batches of EVs were analyzed. Proteins with

relatively higher concentrations are included. **g** Schematics showing the formation of EV gels from azido-labeled EVs and DBCO-PEG via click chemistry. **h** Photos of the mixture of DBCO-PEG and azido-labeled EVs or control EVs at 37 °C. **i** Quantification of EV-N<sub>3</sub> before and after mixing with DBCO-PEG (n=3 technical replicates). **j** Representative plots and **k** average storage moduli (G') and loss Moduli (G") of formed EV gels (n=4 technical replicates). **l** SEM image of EV gels. All the numerical data are presented as mean  $\pm$  SD (two-tailed Student's t test was used;  $0.01 < P \le 0.05; **P \le 0.01; ***P \le 0.001; ****P \le 0.0001$ ).

PEG stays as a solution form at room temperature but rapidly forms a hydrogel upon injection into the body. We further demonstrate that injectable tumor EV hydrogels can serve as a long-term depot for EV-encased tumor antigens, where dendritic cells (DCs) can sample, process, and present the tumor antigens for subsequent priming of tumor-specific CD8<sup>+</sup> T cells (Fig. 1b). After injection, the EV hydrogels are stable for over four weeks in situ, and lead to enhanced humoral and CTL responses than the solution form of EVs. Adjuvants such as CpG oligonucleotides can

also be easily conjugated to EV hydrogels via efficient click chemistry to further tune the CTL response and antitumor efficacy.

# **Metabolic tagging of EVs**

To generate azido-labeled EVs, E.G7-OVA cells were incubated with Ac<sub>4</sub>ManNAz, a commonly used metabolic labeling agent, for three days, followed by the collection of EVs via ultrafiltration (100 kDa MW cutoff) (Fig. 2a). Consistent with previous reports, Ac<sub>4</sub>ManNAz was

able to metabolically label E.G7-OVA cells with azido groups (Supplementary Fig. S1a, b)<sup>53</sup>. To confirm whether azido-labeled E.G7-OVA cells can secrete azido-tagged EVs, EVs from Ac₄ManNAz- or PBS-treated E.G7-OVA cells were incubated with DBCO-Cv5 for 30 min, followed by ultrafiltration to remove unreacted DBCO-Cy5. Compared to control EVs, EVs from Ac<sub>4</sub>ManNAz-treated E.G7-OVA cells showed significantly higher Cy5 fluorescence intensity (Fig. 2b), demonstrating the successful metabolic tagging of EVs with azido groups. By quantifying the fluorescence intensity of conjugated DBCO-Cy5, the surface density of azido groups was estimated to be >4000 per EV (Supplementary Fig. S2). The average size and relative concentration of labeled and unlabeled EVs showed negligible differences, as determined by the Nanoparticle Tracking System (NTA) (Fig. 2c, d, Supplementary Fig. S3a, b). TEM images also confirmed a similar morphology and size distribution between azido-labeled and unlabeled EVs (Fig. 2e). Dynamic light scattering (DLS) confirmed a similar size distribution and a zeta potential of -9.2 mV (Supplementary Fig. S4a, b). -109 purified EVs could be obtained after culturing 1 million E.G7-OVA cells for three days. It is noteworthy that a fraction of EVs may come from FBS in the culture medium, and future studies that aim to obtain purer EVs should involve the removal of EVs from fetal bovine serum (FBS) prior to cell cultures. We also verified the batch-to-batch consistency in harvesting EVs from E.G7-OVA cells (Supplementary Fig. S3c, d). Proteomic analysis confirmed the presence of various types of proteins in EV and azido-labeled EV (Fig. 2f). Also, the protein composition between different batches of EVs was consistent (Fig. 2f). These experiments demonstrated that metabolic glycan labeling of the parent cells can generate chemically tagged EVs without altering the morphology and size of EVs.

# **EV hydrogels with tunable mechanics and gelation temperature**

To fabricate EV hydrogels, we functionalized 8-arm PEG with DBCO (Supplementary Fig. S5), and mixed the synthesized DBCO-PEG (20 mg/mL) with azido-labeled EVs ( $7 \times 10^9/\text{mL}$ ) at 37 °C (Fig. 2g). The mixture rapidly formed a hydrogel as a result of the click reaction between DBCO and azido groups (Fig. 2h). In contrast, the mixture of unlabeled EVs and DBCO-PEG failed to form a hydrogel even after days (Fig. 2h). Indeed, the EV gel showed a high EV capturing efficiency (>99%) during the gel formation process (Fig. 2i). The formed hydrogel has a storage modulus (G') of -13.5 kPa and loss modulus (G'') of -2 kPa (Fig. 2j, k). We also performed SEM imaging of the formed EV hydrogels, which clearly revealed a crosslinked network of nanosized EVs (Fig. 2l). The EVs were tightly packed and formed a nanoporous gel network (Fig. 2l).

To better understand the EV hydrogel system, we next studied the gelation process and mechanical properties of EV gels formed with varying concentrations of azido-labeled EVs. The final concentration of DBCO-PEG was kept at 20 mg/mL, while the final concentration of EVs was set at  $7 \times 10^9$ /mL,  $1.75 \times 10^9$ /mL,  $1.17 \times 10^9$ /mL,  $0.875 \times 10^9$ /mL, and 0.70 × 10<sup>9</sup>/mL for EV gel-1, EV gel-2, EV gel-3, EV gel-4, and EV gel-5, respectively. We first analyzed the gelation temperature of EV hydrogels via dynamic temperature ramp measurements, which showed a decreased gelation temperature for higher EV concentrations (Fig. 3a-c). In particular, EV gel-1 formed at an EV concentration of  $7 \times 10^9$ /mL and DBCO-PEG concentration of 20 mg/mL has a gelation temperature of 39.4 °C (Fig. 3a). This gelation temperature (slightly higher than body temperature) is especially useful for in vivo applications when the mixture of azido-labeled EVs and DBCO-PEG can stay as a solution below the body temperature but forms a gel once injected into the body. By fixing the temperature at 37 °C, higher EV concentrations resulted in more rapid gelation processes and higher storage moduli as expected (Fig. 3d, f). EV gels also exhibited a viscoelastic behavior, with the relaxation half-life increasing with the concentration of EVs (Fig. 3g, h, Supplementary Fig. S6). These experiments demonstrated the tunability of the gelation temperature, gelation time, storage moduli, and relaxation half-lives of EV hydrogels by varying the concentration of azido-labeled EVs. Consistent with the mechanical properties, EV gels with a decreased EV concentration exhibited a higher porosity (Fig. 3i).

# In vitro and in vivo stability of EV hydrogels

We next studied the stability of EV hydrogels. By immersing EV gels in PBS, EV gel-1 showed a ~10% volume loss after 15 days and EV gel-4, which is assumed least stable, showed a ~17% volume loss after 15 days (Fig. 4a-c), demonstrating the overall excellent stability of EV hydrogels in vitro. We also examined the degradation of EV gels in 10% FBS at 37 °C, which showed a 37% volume loss over a course of 21 days for EV gel-1 (Supplementary Fig. S7a-c). To study in vivo stability of EV hydrogels, azido-labeled EVs were conjugated with DBCO-Cy5 and then mixed with DBCO-PEG at room temperature, prior to subcutaneous injection into the flank of Balb/c mice via an 18G needle. Mice were monitored via IVIS imaging for three weeks (Fig. 4d). The mixture of EVs and DBCO-PEG was in a liquid state at room temperature, but rapidly formed a gel-like bulge after injection into the mice. The in situ formed EV gel showed minimal degradation over the first five days, as evidenced by the negligible changes in the gel volume and Cy5 fluorescence intensity (Fig. 4d, f). Over the course of 21 days, EV gels remained stable at the injection site, despite the gradual decrease of gel volume over time (Fig. 4d-f). It is noteworthy that Cy5-conjugated EVs alone, upon subcutaneous injection, were rapidly cleared from the injection site within 2 h (Supplementary Fig. S8). We envision the slow degradation of EV hydrogels would enable the long retention of EV gels while allowing for the gradual release of EV-encased contents over time. Among all gels, EV gel-1 with rapid gelation at 37 °C, favorable mechanical properties, and good stability was used for subsequent experiments.

# In vitro interactions of DCs and EV gels

Next, we studied the interaction between DCs and EV hydrogels, and the processing and presentation of EV gel-encased antigens by DCs. We first confirmed the presence of OVA protein in E.G7-OVA derived EVs via western blot (Fig. 5a). We have also confirmed the presence of Tsg101 and CD63, two common EV markers, in E.G7-OVA derived EVs (Supplementary Fig. S9). Per the ELISA assay, the density of OVA protein was  $2.9 \times 10^{-9} \,\mu g$  per EV. Azido-labeled EVs were mixed with DBCO-PEG at 37 °C for 3 min to form the EV gel. We analyzed the release kinetics of OVA protein from the EV gel by quantifying the released OVA in the culture media at different times using ELISA assay. ~48 ng of OVA was released from EV gels over the course of 14 days (Fig. 5b), which accounts for ~2.3% of the loaded OVA (Fig. 5c), demonstrating the stability of EV gels and sustained release of EV-encased molecules over time. It is noteworthy that OVA shows a burst and much faster release from conventional alginate hydrogel (Supplementary Fig. S10a, b). We also analyzed whether EVs could be released from the EV gels by incubating EV gels in PBS at 37 °C and quantifying the number of particles in PBS over time via NTA. Few particles were detected within 5 days and ~0.5% of initially loaded EVs were detected by day 9 (Supplementary Fig. S11a, b), indicating that the vast majority of EVs remain in the gels and gradually release the encased molecules over time. To assess the interaction between EV gels and DCs, We stained bone marrow-derived DCs (BMDCs) with Calcein AM, added them to the top of the EV gel, and monitored BMDCs and EV gels over time. EV gels remained stable for over 7 days (Fig. 5d-f). BMDCs mostly remained on the surface of the EV gels and exhibited good viability and proliferation over time (Fig. 5e, f). We also confirmed the rapid uptake of EVs, via conjugation of DBCO-Cy5 to azido-labeled EVs, by DCs (Supplementary Fig. S12a). Per confocal imaging, Cy5-conjugated EVs partially overlaid with the early endocytic marker Rab5 at 30 min and late endocytic marker LAMP-1 at 4 h (Fig. 5g). Flow cytometry analysis also confirmed the uptake of Cy5-conjugated EVs by DCs (Supplementary

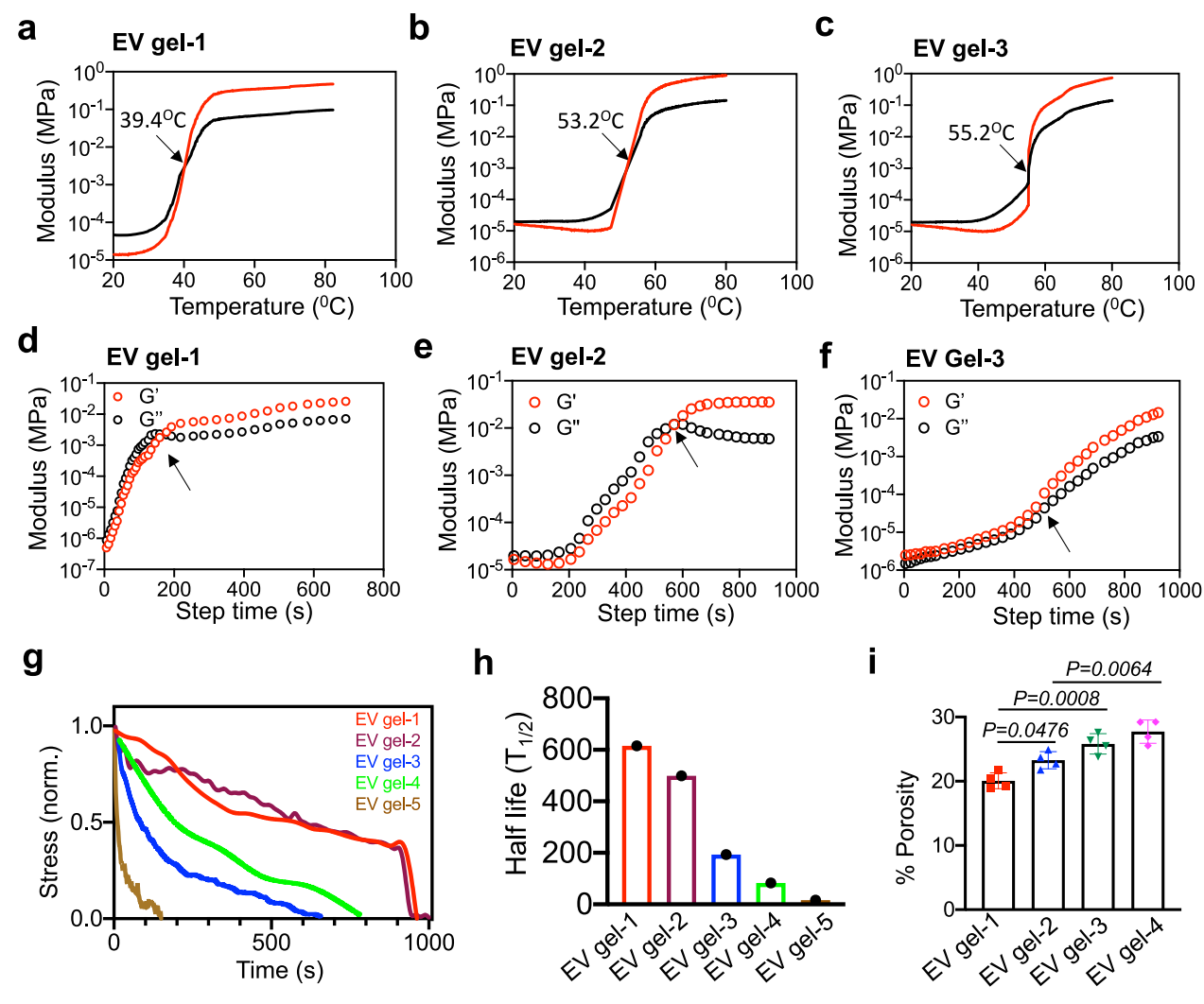


Fig. 3 | EV hydrogels with tunable gelation temperature, storage moduli, and stress relaxation half-lives. EV gels were formed by mixing 8-arm DBCO-PEG and different concentrations of azido-labeled EVs. An EV concentration of  $7 \times 10^9$ /mL,  $1.75 \times 10^9$ /mL,  $1.17 \times 10^9$ /mL,  $0.875 \times 10^9$ /mL, and  $0.70 \times 10^9$ /mL was used for EV gel-1, EV gel-2, EV gel-3, EV gel-4, and EV gel-5, respectively. Shown are the changes of storage moduli (G') and loss moduli (G'') of a EV gel-1, b EV-gel 2, and c EV-gel 3 at

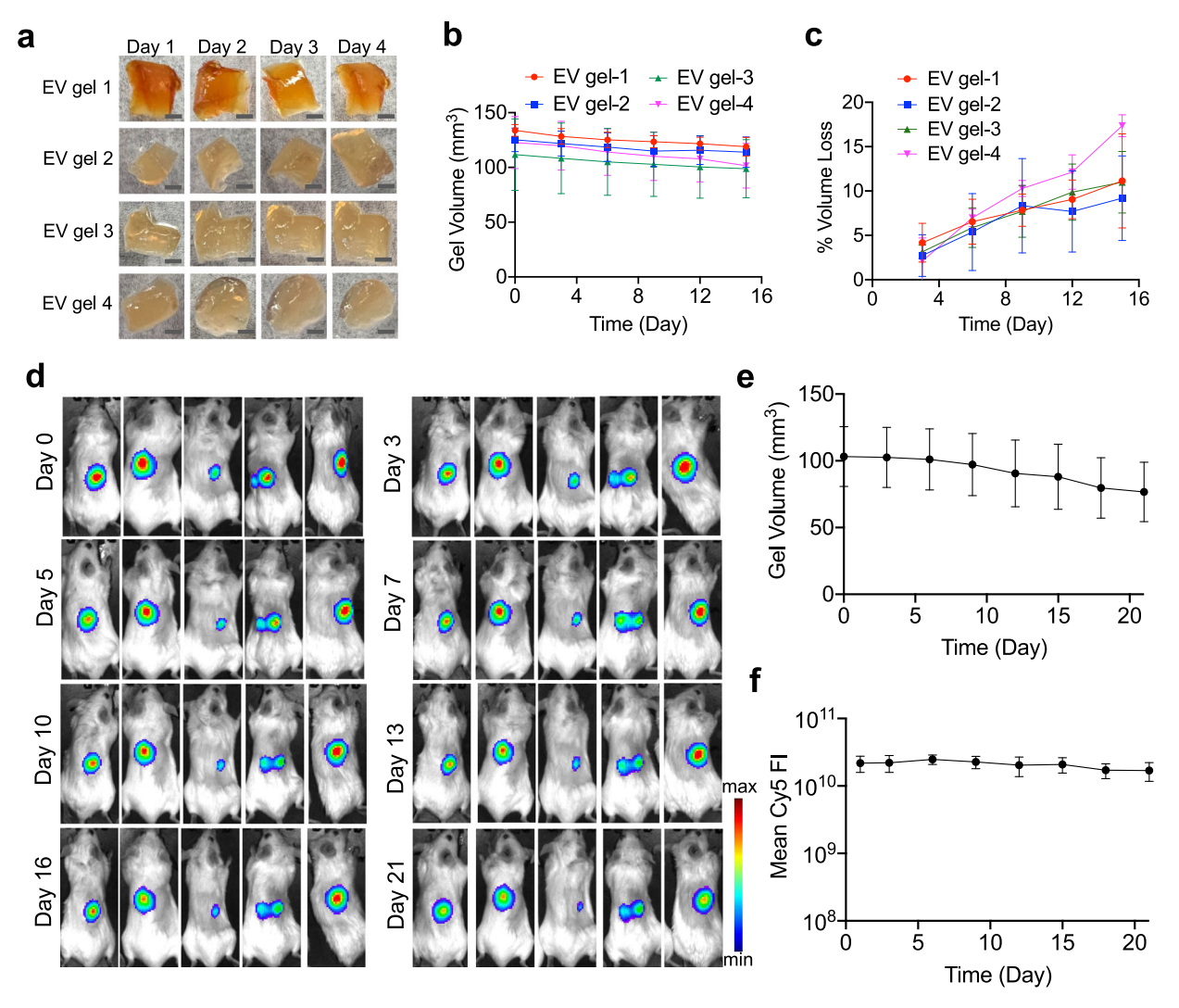
constant strain ( $\gamma$  = 0.5%) during heating from 20 °C to 80 °C, measured at a heating speed of 5 °C/min. Changes of G' and G" over step time at 37 °C for **d** EV gel-1, **e** EV gel-2, and **f** EV gel-3. **g** Representative stress relaxation curves and **h** stress relaxation half-lives of EV gel 1–5. **i** Porosity of EV gels (n = 4 technical replicates, ANOVA with a post hoc Fisher's LSD test was used.  $0.01 < P \le 0.05$ ; \*\* $P \le 0.01$ ; \*\*\* $P \le 0.001$ ; \*\*\* $P \le 0.001$ ).

Fig. S12b). To study DC activation, we seeded BMDCs on top of the EV gel, CpG-encapsulating EV gel (EV gel + CpG), or CpG-conjugated EV gel (EV gel conjugated with DBCO-CpG, denoted as EV/CpG gel), or incubated DCs with a solution of non-crosslinked EVs (with or without CpG). Compared to untreated DCs, DCs treated with EV gels showed an upregulated expression of CD86 (Fig. 5h). The incorporation of CpG, either via physical encapsulation or covalent conjugation, further increased CD86 expression on DCs (Fig. 5h). Compared to the solution of non-crosslinked EVs and CpG, CpG-loaded EV gels showed a similar DC activation effect (Fig. 5h). Similarly, CpG-conjugated EV gels also managed to upregulate the expression of MHCII and MHCI-SIINFEKL complexes on DCs, in comparison with EV gel alone or to the solution of non-crosslinked EVs and CpG (Supplementary Fig. S13a, b). The effect of EV gels on macrophages was also studied by incubating bone marrow-derived macrophages with EV gel, CpG-encapsulating EV gel, CpG-conjugated EV gel, EV alone, or the solution of non-crosslinked EVs and CpG for 16 h, and examining the surface expression of CD163, CD206, and CD86. Compared to the solution of non-crosslinked EVs and CpG, EV gels slightly upregulated the expression of CD163 and CD206 on macrophages (Supplementary Fig. S14a-c). To further understand the interaction of DCs with EV gels, BMDCs were also

loaded into the EV gel, CpG-encapsulating EV gel, or CpG-conjugated EV gel, and incubated for 16 h. Compared to untreated DCs, DCs in EV gels expressed a higher level of CD86, and DCs in CpG-loaded EV gels showed a further increased CD86 expression (Supplementary Fig. S15a-c). It is noteworthy that BMDCs loaded into EV gels showed high viability over time (Supplementary Fig. S16). We next studied whether DCs can process and present E.G7-OVA EV-encased antigens within the hydrogel, BMDCs were loaded into the EV gel, CpGencapsulating EV gel, or CpG-conjugated EV gel, or directly incubated with the solution of OVA and CpG or the solution of EV alone for 16 h, and then co-incubated with CFSE-stained OT-I cells for three days. DCs pretreated with EV gels alone were able to improve the proliferation of OT-I cells compared to non-pretreated DCs (Fig. 5i, j), indicating the uptake and processing of EV-encased OVA antigens by DCs. Consistent with the DC activation result, DCs pretreated with CpG-loaded EV gels induced higher proliferation of OT-I cells than DCs pretreated with EV gel alone (Fig. 5i, j).

# Migration of immune cells to EV gel injection site

We next analyzed the immune cells that migrate to the subcutaneously injected EV gels and the fibrotic tissue surrounding the EV gels. At 3



**Fig. 4** | **EV** hydrogels are stable in vitro and in vivo. a Photos of EV gel 1, EV gel 2, EV gel 3, and EV gel 4 immersed in PBS for different times. An EV concentration of  $7 \times 10^9$ /mL,  $1.75 \times 10^9$ /mL,  $1.17 \times 10^9$ /mL, and  $0.875 \times 10^9$ /mL was used for EV gel-1, EV gel-2, EV gel-3, and EV gel-4, respectively. **b** Change in the volume of gels over time in vitro (n = 4 technical replicates). **c** Percentage of volume loss for EV gels over time in vitro (n = 4 technical replicates). **d**-f Mice were subcutaneously injected with the

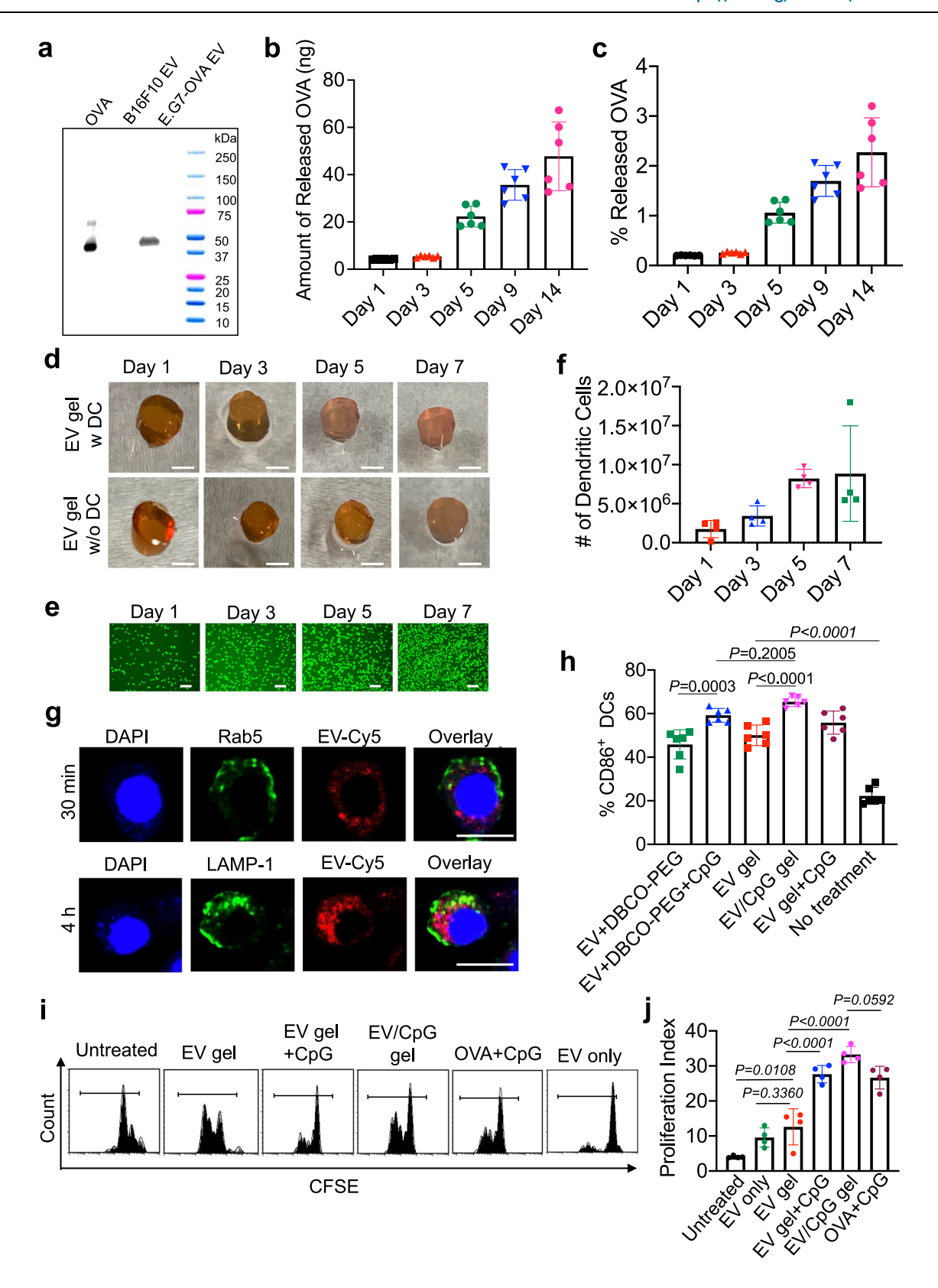
mixture of Cy5-conjugated/azido-labeled EVs and DBCO-PEG, which formed a gel rapidly after injection. **d** IVIS images of mice at different times post injection. **e** Change of EV gel volume over time (n = 5 technical replicates). **f** Change of Cy5 fluorescence intensity of EV gels over time (n = 5 technical replicates). Numerical data are presented as mean  $\pm$  SD.

days post the injection of EV hydrogels, among the CD45<sup>+</sup> population, ~17% were CD11c<sup>+</sup> DCs (Fig. 6a), ~10% were CD11b<sup>+</sup>F4/80<sup>+</sup> macrophages (Fig. 6b), ~10% were CD11b+Gr1+ neutrophils (Fig. 6c), and ~0.5% were CD3<sup>+</sup> T cells (Fig. 6d). Compared to blank EV gels, CpG-conjugated EV gels showed negligible changes in the percentage and number of DCs, macrophages, neutrophils, and T cells at the gel site (Fig. 6a-e, Supplementary Fig. S17a-c). DCs in the EV gels or CpG-conjugated EV gels also expressed a similar level of CD86 and MHCII (Fig. 6f, g). To clarify, most of the immune cells were in the surface layers of the nanoporous EV gels, although a small number of cells might infiltrate into the gels over time. We also analyzed the inflammatory responses at the gel site. At 3 or 7 days post subcutaneous injection of EV gels or CpGconjugated EV gels, a capsule structure surrounding the EV gel was formed (Fig. 6h). On day 3, the capsule tissue surrounding EV/CpG gels showed a similar population of DCs and neutrophils and a slightly higher population of CD4<sup>+</sup> and CD8<sup>+</sup> T cells in comparison with the capsule structure surrounding EV gels (Fig. 6i-k, Supplementary Fig. S18a, b). On day 7, the capsule structure surrounding EV/CpG gels showed a slightly higher population of DCs and neutrophils than the capsule structure surrounding EV gels (Fig. 6l-n). The number of CD4<sup>+</sup>

and CD8<sup>+</sup> T cells showed negligible differences between EV/CpG gel and EV gel (Supplementary Fig. S18c, d). We also measured the cytokine levels at the EV gel injection site on day 3, which showed an increase level of inflammatory cytokines such as TNF-α, IL-16, IL-12, and M-CSF in mice injected with EV/CpG gel or EV gel than untreated mice (Supplementary Fig. S19). The upregulated level of inflammatory cytokines aligns with the infiltration of DCs, neutrophils, and other immune cells (Fig. 6l-n, Supplementary Fig. S18a-d), and likely contribute to the sampling and presentation of EV-encased tumor antigens by antigen presenting cells at the gel site. In a separate study, we also analyzed the blood cells at 3, 6, and 9 days post administration of EV/ CpG gel and EV gel, which showed negligible differences in the number of red blood cells, monocytes, lymphocytes, and granulocytes in comparison with the untreated group (Supplementary Fig. S20a-c), demonstrating the minimal effect of EV gel treatment on blood cell populations.

# **CTL** response of EV gels

After demonstrating the excellent in vivo stability of EV gels and the migration of DCs and other immune cells to the gel site over time, we



next studied whether EV gels can induce antigen-specific CTL response. E.G7-OVA derived EVs were used for this study. C57BL/6 mice were subcutaneously injected with CpG-conjugated EV gel, CpG-encapsulating EV gel, EV gel, the mixture of OVA (50  $\mu$ g) and CpG (50 ng), and PBS, respectively on day 0 (Fig. 7a). Each injected EV gel contained  $7 \times 10^8$  EVs and 2.067  $\mu$ g OVA. Peripheral blood mononuclear cells (PBMCs) were collected at different times for the analysis

of SIINFEKL-specific CD8<sup>+</sup> T cells. On day 6, a higher number of SIINFEKL-specific CD8<sup>+</sup> T cells was detected in mice treated with CpG-conjugated EV gels than in other groups (Fig. 7b, c). EV gels or the mixture of EV gel and CpG also induced a higher frequency of IFN- $\gamma$ <sup>+</sup> CD8<sup>+</sup> T cells, upon ex vivo SIINFEKL restimulation<sup>62</sup>, than the untreated group (Fig. 7c). On day 9, all treatment groups showed a higher number of SIINFEKL-specific CD8<sup>+</sup> T cells than the untreated group

**Fig. 5** | **EV** gels gradually release encased molecules, are biocompatible with **DCs**, and enable the generation of antigen-presenting **DCs** in vitro. a Western blot analysis of OVA in E.G7-OVA derived EVs. Pure OVA protein and EVs collected from B16F10 cells were used as controls. **b**, **c** EV gels (EV gel-1) were incubated at 37 °C for up to 2 weeks. Aliquots of the medium were collected on day 1, 3, 5, 9, and 14, respectively for ELISA assay to quantify the released OVA from EV gels. **b** Accumulated release of OVA from EV gels over time (*n* = 6 technical replicates). **c** Percentage of released OVA over time (*n* = 6 technical replicates). **d**-**f** Calcein AMstained DCs were loaded on top of the EV gel (4 mm diameter × 2 mm height) and incubated at 37 °C. **d** Pictures of EV gels with or without DCs over time. Scale bar: 2 mm. **e** Fluorescence images of DCs on EV gels at different times. Scale bar: 100 μm. **f** Quantification of DCs on EV gels over time (*n* = 4 technical replicates). '#' denotes number. **g** CLSM images of DCs after incubation with EV-Cy5 for 30 min and 4 h, respectively. DCs were stained with Rab5 primary antibody and FITC-

conjugated goat anti-rabbit secondary antibody, or Alexa Fluor 488-conjugated anti-LAMP-1. Scale bar:  $10~\mu m$ . This experiment was repeated independently at least three times with similar results. **h** Percentages of CD86<sup>+</sup> DCs after incubation with different groups for 16 h (n=6 technical replicates). DCs were added to the top of EV gels (EV gel, CpG-conjugated EV gel, or CpG-encapsulating EV gel) or incubated with the solution of non-crosslinked EVs (without or with CpG). **i, j** DCs were loaded into EV gel, CpG-encapsulating EV gel, CpG-conjugated EV gel, or incubated with a solution of OVA and CpG or the solution of EVs for 16 h, harvested, and then cocultured with CFSE-stained OT-I cells for three days. Shown are (**i**) representative CFSE histograms of OT-I cells and (**j**) proliferation index of OT-I cells in different groups (n=4 technical replicates). All the numerical data are presented as mean  $\pm$  SD (ANOVA with a post hoc Fisher's LSD test was used.  $0.01 < P \le 0.05$ ; \*\* $P \le 0.01$ ; \*\*\* $P \le 0.001$ ; \*\*\* $P \le 0.001$ ; \*\*\* $P \le 0.0001$ ).

(Fig. 7d, e, Supplementary Fig. S21a, b). Compared to EV gel alone or CpG-encapsulating EV gel, CpG-conjugated EV gels consistently induced a higher frequency of SIINFEKL-specific CD8+ T cells62 in PBMCs on days 9 and 14 (Fig. 7d–g, Supplementary Fig. S21a, b). In the subsequent prophylactic tumor study, all EV gel groups exhibited slower tumor growth than the untreated group (Fig. 7h). Compared to EV gel alone, CpG-conjugated EV gels resulted in slower tumor growth (Fig. 7h). It is noteworthy that EV gel treatment did not induce any noticeable toxicity to healthy tissues including spleen, liver, kidney, heart, and lungs (Supplementary Fig. S22). These experiments demonstrated that CpG-conjugated EV gels can effectively modulate the DCs that arrive at the gel site and facilitate the processing and presentation of EV-encased antigens by DCs, thereby enhancing the antigen-specific CTL response.

# Antitumor efficacy and antibody response of EV gel vaccines

After demonstrating the enhanced CTL response and prophylactic antitumor efficacy of CpG-conjugated EV hydrogels, we next evaluated their therapeutic antitumor efficacy and potential synergy with anti-PD-1 checkpoint blockade. C57BL/6 mice were inoculated with E.G7-OVA tumors on day 0 and divided into 5 groups: the combination of CpG-conjugated EV gel and anti-PD-1, CpG-conjugated EV gel, EV gel, anti-PD-1, and PBS (Fig. 8a). EV gels were subcutaneously injected into the flank of mice on day 9, while anti-PD-1 was injected on days 13, 16, and 19, respectively (Fig. 8a). All treatment groups managed to slow down the growth of tumors in comparison with the untreated group (Fig. 8b). Compared to CpG-conjugated EV gel alone or anti-PD-1 alone, the combination of CpG-conjugated EV gel and anti-PD-1 led to an improved tumor control (Fig. 8c). These experiments demonstrated the promise of EV gel-based cancer vaccines to induce enhanced CTL response and antitumor efficacy, and the synergistic effect between EV gel vaccines and checkpoint blockades. As a proof-of-concept demonstration, we also evaluated the promise of the EV gel to induce long-term humoral responses. C57BL/6 mice were injected with CpG-conjugated EV gels, EV gels, or the mixture of EVs and CpG on day 0, followed by the analysis of anti-OVA titers in the serum at different times. At all examined times (days 5, 7, 12, and 18), EV gels consistently generated higher anti-OVA titers than the bonus mixture of EV and CpG (Fig. 8d-g). Compared to EV gels, CpG-conjugated EV gels showed further increased anti-OVA titers from day 12 (Fig. 8d-g).

To understand the alteration of the tumor microenvironment as a result of EV gel treatment, mice bearing E.G7-OVA tumors were treated with CpG-conjugated EV gel, CpG-encapsulating EV gel, EV gel, the mixture of OVA ( $50\,\mu g$ ) and CpG ( $50\,n g$ ), EV alone, the mixture of EV, DBCO-PEG and CpG, and PBS, respectively. Tumors were harvested at 3 days post gel injection for immune cell analysis (Fig. 9a). Compared to EV gel or other groups, CpG-conjugated EV gel resulted in an increase in the number of intratumoral CD3 $^+$  T cells and CD8 $^+$  T cells (Fig. 9b–d), along with an upregulated expression of CD69 on the

surface of intratumoral CD8+ T cells (Fig. 9e). CpG-conjugated EV gel also decreased the number of intratumoral regulatory T cells (Tregs) (Fig. 9f), increased the CD8<sup>+</sup> T/Treg number ratio (Fig. 9g), increased the number of intratumoral DCs (Fig. 9h), and upregulated the expression of CD86 on the surface of intratumoral DCs (Fig. 9i), in comparison with EV gel, EV alone, the mixture of non-crosslinked EVs, DBCO-PEG and CpG. We also examined the expression of CTLA-4, PD-1, and LAG-3 exhaustion markers on the surface of CD8+ T cells in the tumor (Fig. 9k-m). Compared to EV gel or no treatment group, CpGconjugated EV gels resulted in a slightly increased expression of CTLA-4 and LAG-3 on intratumoral CD8<sup>+</sup> T cells (Fig. 9k-m). These experiments demonstrated the ability of CpG-conjugated EV gels to reprogram the immunosuppressive tumor microenvironment. We also analyzed the immune cells in the gel and surrounding skin tissues. Compared to EV alone or untreated group, CpG-conjugated EV gels increased the number of CD8<sup>+</sup> T cells, CD4<sup>+</sup> T cells, CD69<sup>+</sup>CD8<sup>+</sup> T cells, CD11c<sup>+</sup> DCs, CD86<sup>+</sup> DCs, and F4/80<sup>+</sup> macrophages at the injection site (Supplementary Fig. S23a-g). CpG-conjugated EV gels also resulted in a higher number of CD11c<sup>+</sup> DCs, CD86<sup>+</sup>CD11c<sup>+</sup> DCs, and F4/80<sup>+</sup> macrophages than EV gels (Supplementary Fig. S23e-g).

# **Discussion**

Here we present an EV-based hydrogel system in which nanosized EVs serve as the multifunctional backbone to form the crosslinked gel network. The gelation temperature, gelation rate, storage and loss moduli, and relaxation time of the formed EV gel can be fine-tuned by adjusting the concentration of EVs. Our strategy is different from conventional approaches that physically encapsulate EVs in an existing hydrogel network, and enable the fabrication of EV-based gels with excellent stability and tunable mechanics and injectability. One such EV hydrogel, formed with an EV concentration of  $7 \times 10^9$ /mL and DBCO-PEG concentration of 20 mg/mL, has a gelation temperature of 39.4 °C that is close to the body temperature. We showed that the mixture of azido-labeled EVs and DBCO-PEG stayed as a liquid at room temperature but could rapidly form a crosslinked gel within 3 min at 37 °C. Similarly, when subcutaneously injected into the flank of mice, the mixture immediately formed a bulge at the injection site and remained as an intact gel even after weeks. These EV hydrogels can function as a long-term depot of EVs and EV-encased molecules for various applications.

We anticipate that the EV tagging and crosslinking approach can be universally applied to various types of cells including stem cells, immune cells, and bacteria, for the fabrication of corresponding EV gels. The injectable and mechanically tunable EV gels could serve as a long-term depot of EVs and EV-encased molecules for a variety of applications. For example, EV gels derived from mesenchymal stem cells could find promising applications in regenerative medicine and immunosuppression. EV gels derived from bacteria could serve as a long-lasting vaccine for the prevention and treatment of bacterial infections.

In the context of tumor EV vaccines, we show that the subcutaneously injected EV gels can serve as a stable depot for EVs and EV-

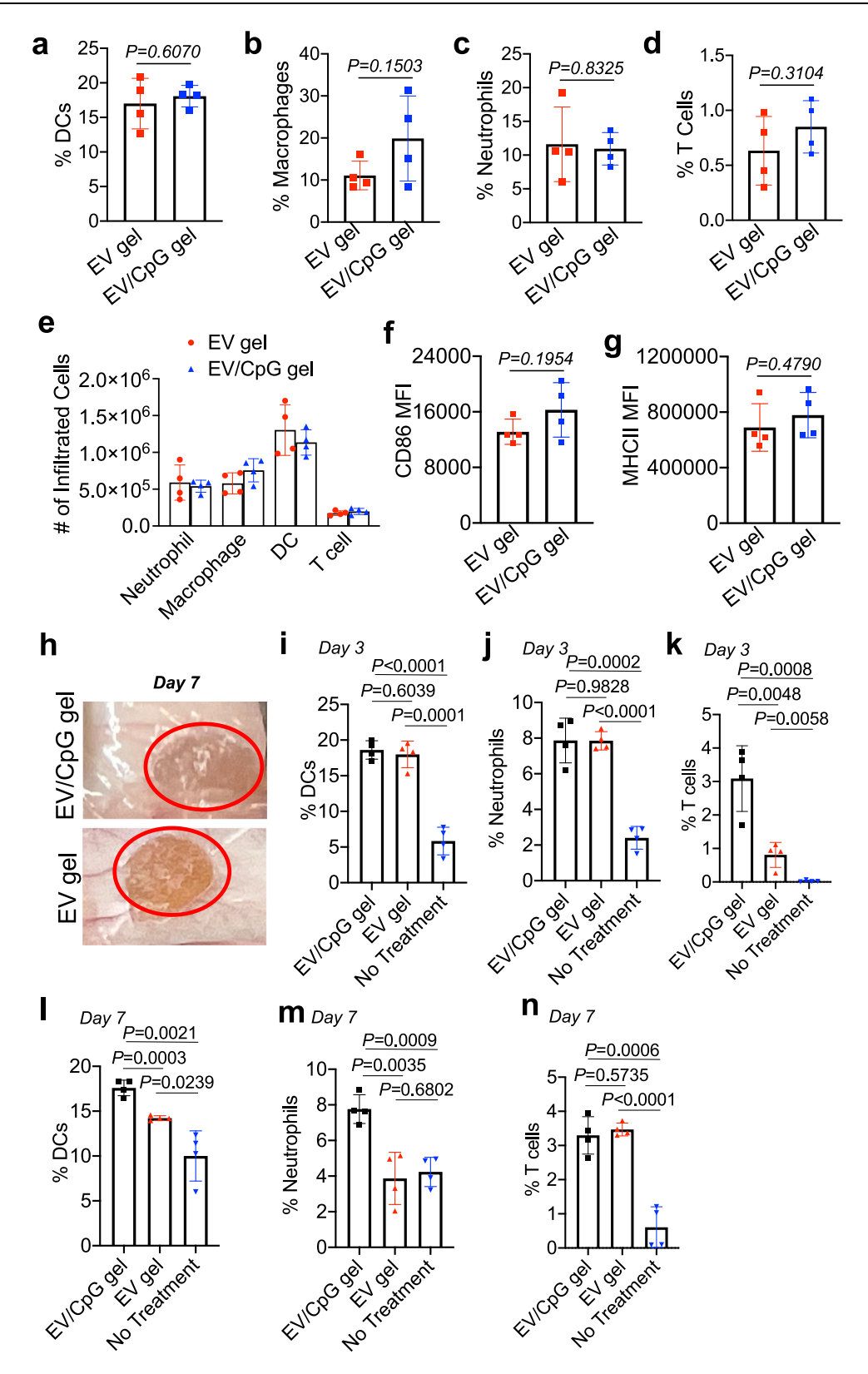


**Fig. 6** | **Immune cells including DCs migrate to subcutaneously injected EV gels.** Mice were subcutaneously injected with the mixture of azido-labeled EVs (with or without conjugation of DBCO-CpG) and DBCO-PEG, which formed gels rapidly after injection. Gels were harvested after three days. Shown are percentages of **a** DCs, **b** macrophages, **c** neutrophils, and **d** T cells among CD45<sup>+</sup> cells at the gel site (n = 4 mice). **e** Number of neutrophils, macrophages, DCs, and T cells at the gel site (n = 4 mice). '#' denotes number. **f** CD86 MFI of DCs at the gel site (n = 4 mice). **g** MHCII MFI

of DCs at the gel site (n = 4 mice). **h** Pictures of EV/CpG gel and EV gel at 7 days after subcutaneous injection. Also shown are the percentages of **i** DCs, **j** neutrophils, and **k** T cells in the fibrous capsule surrounding the gel at 3 days post gel injection (n = 4 mice). Percentages of **l** DCs, **m** neutrophils, and **n** T cells in the fibrous capsule surrounding the gel at 7 days post gel injection (n = 4 mice). All the numerical data are presented as mean  $\pm$  SD (two-tailed Student's t test was used.  $0.01 < P \le 0.05$ ;  $P \le 0.01$ ;  $P \le 0.001$ ;  $P \le 0.001$ ;  $P \le 0.001$ ;  $P \le 0.0001$ .

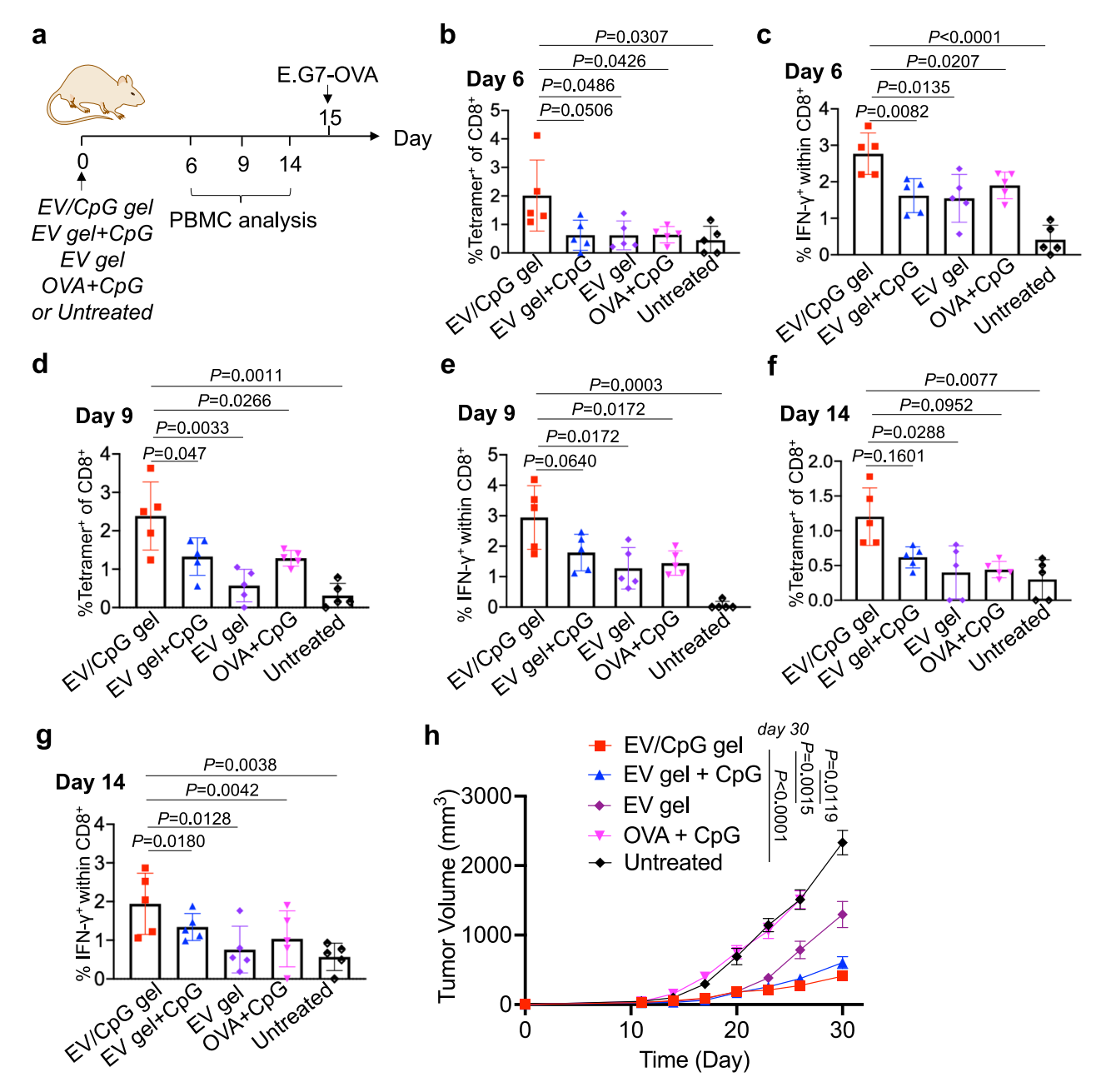


**Fig. 7** | **CpG-conjugated EV gels exhibit enhanced CTL response and antitumor efficacy. a** Timeframe of the vaccination study. EV gel, EV gel+CpG, EV/CpG gel, OVA+CpG or PBS were subcutaneously injected into C57BL/6 mice on day 0. E.G7-OVA tumor cells were inoculated on day 15. Shown are the percentages of (**b**, **d**, **f**) MHCI-SIINFEKL tetramer\* CD8\* T cells and (**c**, **e**, **g**) IFN-r\* CD8\* T cells (after ex vivo SIINFEKL restimulation) in PBMCs on day 6, 9, and 14, respectively (n = 5 mice).

**h** Average E.G7-OVA tumor volume of each group over the course of the prophylactic tumor study (n = 5 mice). Statistical analyses on day 30 are provided. All the numerical data are presented as mean  $\pm$  SD except for (**h**) where data are presented as mean  $\pm$  SEM (ANOVA with a post hoc Fisher's LSD test was used.  $0.01 < P \le 0.05$ ; \*\* $P \le 0.01$ ; \*\*\* $P \le 0.001$ ; \*\*\* $P \le 0.001$ ).

encased tumor antigens, providing an extended time for the modulation of antigen presenting cells (e.g., DCs). Compared to the mixture of OVA and CpG, EV hydrogels fabricated from E.G7-OVA-derived EVs resulted in improved tumor control. EV gels also enable the conjugation of immunomodulatory agents such as CpG adjuvant for further amplification of CTL response and antitumor efficacy. Compared to EV gel alone, CpG-conjugated EV gels resulted in durable CTL response and improved tumor control in both prophylactic and therapeutic settings. In addition, CpG-conjugated EV gels showed a synergistic effect with anti-PD-1 checkpoint blockade for cancer treatment. These studies demonstrated the great promise of our EV hydrogel system for vaccination applications. In previously explored EV-based vaccines, EVs are largely administered in a free form and are expected to traffic

to DCs in the lymphatic tissues for subsequent T cell priming processes, which inevitably suffers from a low efficiency<sup>49–52,54,55</sup>. Our injectable EV hydrogel system provides an alternative approach by forming stable EV depots for sustained in situ modulation of DCs and elicitation of antigen-specific T cell response.

To conclude, we have developed EV hydrogels with tunable viscoelasticity and injectability, by metabolically tagging EVs with azido groups and crosslinking them with DBCO-PEG via click chemistry. Upon subcutaneous injection, the EV hydrogel gel can be rapidly formed in situ and are stable for over 4 weeks, with the gradual attraction of immune cells including DCs. EV gels can induce the activation of DCs and facilitate the processing and presentation of EVencased antigens by DCs, resulting in improved tumor control than

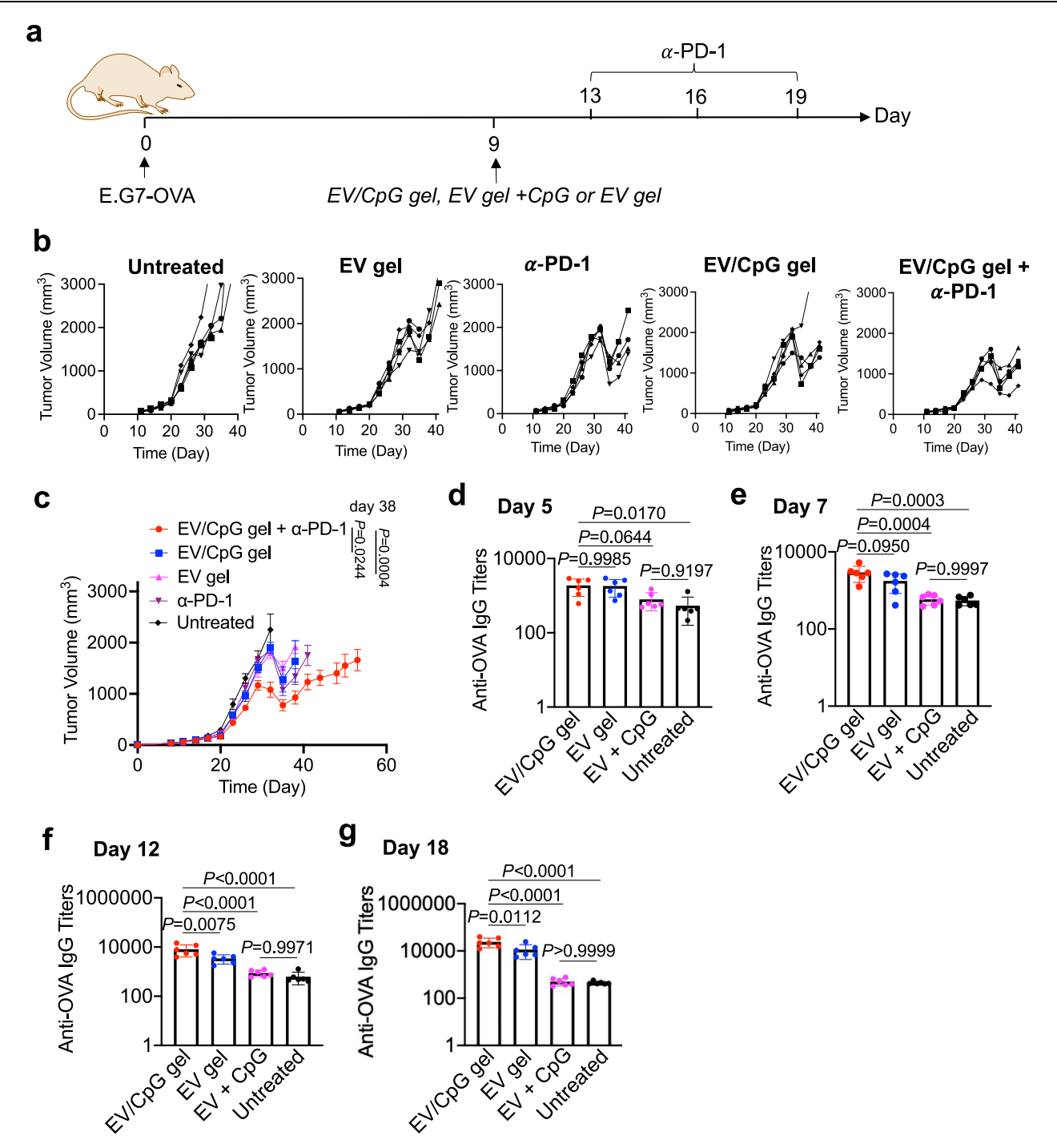


**Fig. 8** | **CpG-conjugated EV gel shows synergy with α-PD-1 for tumor treatment and induces enhanced antibody responses. a** Timeframe of the therapeutic tumor study against E.G7-OVA tumors for ( $\mathbf{a}$ – $\mathbf{d}$ ). E.G7-OVA tumor was inoculated on day 0. EV/CpG gel or EV gel was subcutaneously injected on day 9. α-PD-1 was i.p. administered on days 13, 16 and 19. b Individual tumor curves for each group. **c** Average E.G7-OVA tumor volume of each group over the course of the therapeutic tumor study (n = 5 mice). Statistical analyses on day 38 are provided.  $\mathbf{d}$ – $\mathbf{g}$  C57BL/6

mice were subcutaneously injected with EV/CpG gel, EV gel, the mixture of uncrosslinked EV and CpG, or PBS on day 0. Shown are the anti-OVA lgG titers in the serum of mice on  $\bf d$  day 5,  $\bf e$  day 7,  $\bf f$  day 12, and  $\bf g$  day 18, respectively (n=6 mice). Anti-OVA titers were measured via ELISA assay. Data in ( $\bf c$ ) are presented as mean  $\pm$  SEM and data in ( $\bf d$ - $\bf g$ ) are presented as mean  $\pm$  SD (ANOVA with a post hoc Fisher's LSD test was used.  $0.01 < P \le 0.05$ ; \*\* $P \le 0.01$ ; \*\*\* $P \le 0.001$ ; \*\*\* $P \le 0.0001$ ).

bolus vaccines. The covalent conjugation CpG to EV gels further improves the CTL response and antitumor efficacy. We also demonstrate the synergistic effect between CpG-conjugated EV gels and anti-PD-1 checkpoint blockade for cancer treatment. This EV hydrogel system provides a unique approach to amplifying the humoral and T cell responses towards EV-encased antigens and improving the therapeutic efficacy of EV-based therapies.

# Methods

# **Materials and instrumentation**

We purchased 8-Arm PEG-amine (20 kDa) from JenKem Technology USA (Plano, TX, USA), DBCO-NHS from Click Chemistry Tools (Scottsdale, AZ, USA), Ovalbumin (OVA) protein from InvivoGen (San Diego, CA, USA), DBCO compounds from Sigma Aldrich (St. Louis, MO, USA), and Ovalbumin Polyclonal Antibody HRP, goat anti-mouse-IgG

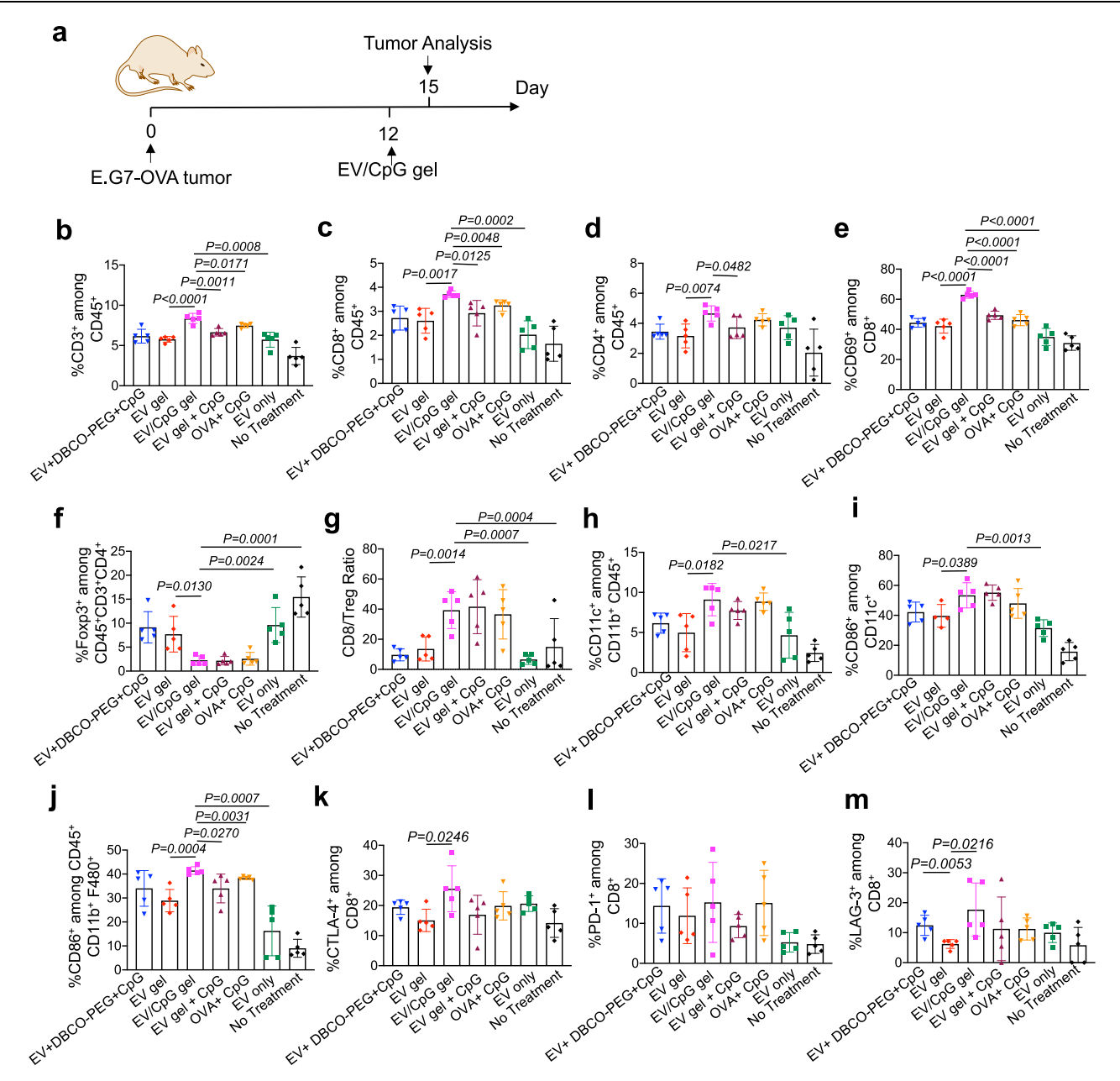


**Fig. 9** | **CpG-conjugated EV gel reprograms the tumor microenvironment.** E.G7-OVA tumor was inoculated to C57BL/6 mice on day 0, followed by the subcutaneous injection of CpG-conjugated EV gel (EV/CpG gel), CpG-encapsulating EV gel, EV gel, the solution of OVA and CpG, EV alone, the non-crosslinked solution of EV, DBCO-PEG and CpG, or PBS on day 12. Tumors were harvested for analysis on day 15. **a** Timeframe of immune cell analysis study. **b** % CD3<sup>+</sup> cells among CD45<sup>+</sup> population (n = 5 mice). **c** % CD8<sup>+</sup> cells among CD45<sup>+</sup> population (n = 5 mice). **d** % CD4<sup>+</sup> cells among CD45<sup>+</sup> population (n = 5 mice). **e** % CD69<sup>+</sup> cells among CD8<sup>+</sup>

population (n=5 mice). **f** % FoxP3\* cells among CD45\*CD3\*CD4\* population (n=5 mice). **g** Number ratio of CD8\* T cells to Tregs (n=5 mice). **h** % CD11c\* DCs among CD11b\*CD45\* population (n=5 mice). **i** % CD86\* cells among CD11c\* DCs (n=5 mice). **j** % CD86\* cells among CD11b\*F4/80\* macrophages (n=5 mice). **k** % CTLA-4\* cells among CD8\* T cells (n=5 mice). **l** % PD-1\* cells among CD8\* T cells (n=5 mice). **m** % LAG-3\* cells among CD8\* T cells (n=5 mice). All the numerical data are presented as mean  $\pm$  SD (ANOVA with a post hoc Fisher's LSD test was used. 0.01 <\* $P \le 0.05$ ; \*\* $P \le 0.01$ ; \*\*\* $P \le 0.001$ ; \*\*\* $P \le 0.001$ ; \*\*\* $P \le 0.0001$ ).

secondary antibody, HRP-conjugated streptavidin from Thermo Fisher Scientific (Waltham, MA, USA). Primary antibodies including fluorophore conjugated anti-CD45, anti-CD11b, anti-CD11c, anti-CD86, anti-MHCII, anti-CD3, anti-CD4, anti-CD8, anti-Gr-1, anti-F4/80, anti-TER119, anti-CD15, anti-CD41, anti-Ly6C, anti-PD-1, anti-CTLA-4, anti-LAG-3, and anti-FoxP3 were obtained from Thermo Fisher Scientific (Waltham, MA, USA). qEV isolation columns were purchased from IZON Science (Christchurch, New Zealand). Mouse CD3<sup>+</sup>T cell isolation kit, dynabeads, and LS separation columns were purchased from Miltenyi Biotec (Bergisch Gladbach, Germany). FACS analyses were performed on an Attune NxT. The fluorescence intensity

of solutions and cells was measured using a BioTek plate reader (Winooski, Vermont, U.S.). Small molecules were characterized using the Shimadzu LC40 ultra high-performance liquid chromatography/mass spectrometer. Proton nuclear magnetic resonance spectra were collected on the Varian U500 or VXR500 (500 MHz) spectrometer. Scanning electron microscopic (SEM) images were taken with a Hitachi S-4800 High Resolution Scanning Electron Microscope. Mechanical tests were performed on an AR-G2 rheometer (TA Instruments, New Castle, DE, USA). The size and size distribution of EVs were measured on a Nanoparticle Tracking Analysis (NTA) system (Malvern, United Kingdom).

#### Cell lines and animals

The E.G7-OVA cell line was purchased from American Type Culture Collection (Manassas, VA, USA). Cells were cultured in DMEM containing 10% FBS, 100 units/mL Penicillin G, 100  $\mu$ g/mL streptomycin, and 50  $\mu$ g/mL G418 at 37 °C in 5% CO2 humidified air. Female C57BL/6 and OT-1 mice were purchased from the Jackson Laboratory (Bar Harbor, ME, USA). All procedures involving animals were done in compliance with National Institutes of Health and Institutional guidelines with approval from the Institutional Animal Care and Use Committee at the University of Illinois at Urbana-Champaign (IACUC protocol number 23201).

#### Synthesis of Ac<sub>4</sub>ManNAz

Ac<sub>4</sub>ManNAz was synthesized following a previously reported method<sup>50,51</sup>. In brief, D-Mannosamine hydrochloride (10.0 mmol) and triethylamine (11.0 mmol) were dissolved in methanol (100 mL), followed by the addition of N-(2-azidoacetyl) succinimide (11.0 mmol) in methanol (5 mL). After stirring at room temperature for 24 h, the solvent was removed and the residue was re-dissolved in pyridine (100 µL). Acetic anhydride (10 mL) was then added and stirred at room temperature for another 24 h. The crude product was purified by silica gel column chromatography using ethyl acetate/hexane (1/1, v/v) as the eluent to yield a white solid (1/1  $\alpha/\beta$  isomers). The final compound was characterized using <sup>1</sup>H and <sup>13</sup>C NMR spectrometry and mass spectrometry. <sup>1</sup>H NMR (CDCl<sub>3</sub>, 500 MHz): δ (ppm) 6.66&6.60 (d, J = 9.0 Hz, 1H, C(O)NHCH), 6.04&6.04 (d, 1H, J = 1.9 Hz, NHCHCHO), 5.32-5.35&5.04-5.07 (dd, J = 10.2, 4.2 Hz, 1H,  $CH_2CHCHCH$ ), 5.22&5.16 (t, J = 9.9 Hz, 1H, CH<sub>2</sub>CHCHCH), 4.60-4.63&4.71-4.74 (m, 1H, NHCHCHO), 4.10-4.27 (m, 2H, CH<sub>2</sub>CHCHCH), 4.07 (m, 2H, C(O)CH<sub>2</sub>N<sub>3</sub>), 3.80-4.04 (m, 1H, CH<sub>2</sub>CHCHCH), 2.00-2.18 (s, 12H, CH<sub>3</sub>C(O)). <sup>13</sup>C NMR (CDCl<sub>3</sub>, 500 MHz): δ (ppm) 170.7, 170.4, 170.3, 169.8, 168.6, 168.3, 167.5, 166.9, 91.5, 90.5, 73.6, 71.7, 70.5, 69.1, 65.3, 65.1, 62.0, 61.9, 52.8, 52.6, 49.9, 49.5, 21.1, 21.0, 21.0, 20.9, 20.9, 20.9, 20.8. ESI MS (*m/z*): calculated for C<sub>16</sub>H<sub>22</sub>N<sub>4</sub>O<sub>10</sub>Na [M+Na]<sup>+</sup> 453.1, found 453.1.

# Flow cytometry analysis of cells

Cells were incubated with Ac<sub>4</sub>ManNAz (50  $\mu$ M) or PBS for 3 days. After washing, cells were incubated with DBCO-Cy5 (10  $\mu$ M) for 30 min and were further washed prior to analysis on a flow cytometer.

#### EV isolation and characterization

E.G7-OVA cells (1×10<sup>6</sup>) were cultured in the presence of Ac<sub>4</sub>ManNAz (50 μM) or PBS for 3 days. The cell culture media was collected on days 4 or 5, after which it was subjected to initial centrifugation at  $350 \times g$ for 5 min to remove cell debris and larger particles. The supernatant was then collected and further purified using ultrafiltration. An Amicon filter with a 100 kDa molecular weight cutoff was used for the ultrafiltration to remove all molecules with molecular weights lower than 100 kDa. The ultrafiltration was conducted using centrifuge 5910 Ri (Eppendorf) at  $4347 \times g$  for 40 min. At least 5 ultrafiltration washing steps (using PBS,  $4347 \times g$ , 40 min) were performed to purify EVs. The size and concentration of EVs were determined on the NTA instrument. For the NTA, we used the Malvern NanoSight NS300 instrument. The measurement volume was 500 µL. The length of the video was 10 secs each and the number of videos taken was 5 per sample. The instrument settings has been listed below: [Capture Settings: Camera Type: sCMOS; Laser Type: Blue488; Camera Level: Manual settings used; Slider Shutter: 1300; Slider Gain: 512; FPS 25.0; Number of Frames: 1498; Temperature: 22.5-22.5 °C; Viscosity: (Water) 0.941-0.942 cP; Dilution factor: Dilution not recorded; Syringe Pump Speed: 100. Analysis Settings: Detect Threshold: 17; Blur Size: Auto; Max Jump Distance: Auto: 2.0–14.8 pix]. To validate the presence of azido groups on the surface of EVs, EVs derived from Ac<sub>4</sub>ManNAz-treated E.G7-OVA cells were incubated with DBCO-Cy5 (10 µM) for 30 min, washed with PBS via ultrafiltration (100 kDa Amicon filter,  $4347 \times g$ , 40 min), and the Cy5 fluorescence intensity was measured on a plate reader.

#### Uptake of EVs by DCs

DC 2.4 cells were seeded onto coverslips in a 6-well plate at a density of  $6\times10^6$  cells per well and allowed to attach for 48 h. Cy5-conjugated EVs (synthesized via the conjugation of EV-N3 and DBCO-Cy5) or control EVs were incubated with DC 2.4 cells at 37 °C for 1 h. After washing with PBS, cells were fixed with 4% paraformaldehyde solution, followed by the staining of cell nuclei and membrane with DAPI (blue) and cell mask stain (green), respectively. The coverslips were mounted onto microscopic slides with Prolong-gold and imaged under a confocal laser scanning microscope.

#### **TEM imaging of EVs**

Isolated EVs were added onto formvar/carbon-coated TEM grids (Ted Pella, Redding, CA), allowed to dry, negatively stained with 2% aqueous uranyl acetate, and imaged with a JEOL 2100 TEM at 200 kV.

#### **Fabrication of EV gels**

E.G7-OVA cells (1 × 10<sup>6</sup>) were metabolically labeled with Ac<sub>4</sub>ManNAz for three days, for subsequent secretion of azido-labeled EVs. Purified azido-labeled EVs (7 × 10<sup>9</sup>/mL, 1.75 × 10<sup>9</sup>/mL, 1.17 × 10<sup>9</sup>/mL, 0.875 × 10<sup>9</sup>/mL, or 0.7 × 10<sup>9</sup>/mL final concentration) were then mixed with 8-arm DBCO-PEG (20 mg/mL final concentration) for 3 min at 37 °C to form EV gels. For some experiments, CpG adjuvant was incorporated into the EV gel by either conjugating azido-labeled EVs with DBCO-modified CpG and further mixing with 8-arm DBCO-PEG to form the crosslinked EV/CpG Gel, or physically encapsulating CpG into EV gels.

#### **Porosity measurement**

EV gels were first placed in DI water for 1-2 h. EV gels were then placed on a Kimwipe paper to dry one side of the gel, so that the water inside the pores can come out through capillary action. The weight of gels before and after the wicking assay was measured, and the porosity of the gel was calculated as  $(W_i$ - $W_f$ )/ $W_i$ .

# Gel volume analysis

EV gels were placed in the medium for 2 weeks at ambient temperature. The length and width of gels were monitored at different times, and the volume of gels was calculated via  $V = (W^2xL)/2$ .

# EV measurement before and after EV gel formation

Initially, EVs were suspended in PBS, and the concentration of EVs in PBS was measured using the Nanoparticle Tracking Analysis (NTA) instrument. EVs in PBS were then mixed with DBCO-PEG to form the gel. After the EV gel was formed, the remaining PBS solution that did not incorporate into the gel was collected, and the gel was washed with fresh PBS. The combined PBS solutions were analyzed by the NTA to measure the concentration of EVs. The total number of EVs was calculated by multiplying the concentration of EVs and the volume of EV solution.

#### In vitro T cell proliferation Assay

EV gel, EV gel+ CpG, EV gel/CpG, and OVA+CpG were placed in a 96-well plate containing 50k DCs per well. 100 k CFSE-stained OT-I cells were added to the surface of the gel, allowing gels to absorb the T cell-containing medium. Finally, T cell medium without IL-2 was added and incubated for 3 days prior to the flow cytometry analysis.

#### In vivo stability of EV gels

Azido-labeled EVs were incubated with DBCO-Cy5 for 30 min, and washed with PBS via ultrafiltration ( $4347 \times g$ , 40 min) with an Amicon centrifugal filter (100 kDa). Then, EV gels were formed in vivo by injecting the mixture of Cy5 conjugated azido-labeled EVs with DBCO-PEG into the flank of Balb/c mice. IVIS imaging was used to monitor the release of Cy5-conjugated EVs at different time points.

#### Immune cell profile of EV gels

C57BL/6 mice were subcutaneously injected with the mixture of azidolabeled EVs and DBCO-PEG. Gels were isolated from mice after 3 days, disrupted, and passed through a 40 µm strainer to collect the cells. Cells were then washed with PBS, stained with fluorophore-conjugated antibodies, and run on a flow cytometer.

#### Interaction of BMDCs with EV gels

Bone marrow-derived DCs were stained with Calcein AM (10  $\mu$ M) for 30 min and washed twice with PBS. After washing, cells were added to the top of the EV gel (4 mm diameter  $\times$  2 mm height) and incubated at 37 °C. The viability and proliferation of DCs on top of the gel were monitored over a week using fluorescence microscopy. Pictures of EV gels were taken over time.

#### Mechanical characterization of EV gels

All tests were performed on an AR-G3 rheometer (TA Instruments) using a 20 mm plate (1.4 mm thickness). The strain sweep test was performed under 0.1–100% strain at a frequency of 1 Hz to determine the linear viscoelastic region of EV gels at different temperatures to ensure that the strain value falls within the linear elastic region. No prestress or pressure was applied to the EV gels during the measurement. Solutions of azido-labeled EVs and DBCO-PEG were mixed right before depositing onto the surface plate of the rheometer for the measurement of gelation temperature and time. The gelation temperature of hydrogels for different concentrations of EVs was measured via oscillatory temperature ramp rheological experiments. The storage and loss moduli of formed EV gels were measured by running the time sweep test at 0.5% strain and 1 Hz frequency under room temperature. The viscosity of hydrogels was determined using the flow sweep test performed at 0.5% strain. The stress relaxation of gels was evaluated by subjecting gels to a constant 15% strain.

#### Release of OVA from EV gel

EV gels ( $7 \times 10^8$  EVs) were incubated at 37 °C for up to 2 weeks in a 48-well plate.  $200\,\mu$ L aliquots of media were collected on days 1, 3, 5, 9, and 14, and sampled for ELISA assay to quantify the released OVA from EV gels.

#### **Proteomic analysis**

EVs were collected and purified via ultrafiltration with an Amicon centrifugal filter (100 kDa) and qEV column. Reduction, alkylation of cysteines, and sequential digestion by LysC and trypsin were performed followed by StageTip desalting. Proteins were analyzed on an LC-MS by a trained staff in the Proteomic Analysis Core.

# Western blot analysis of EVs

EVs were obtained from E.G7-OVA cell culture medium, with or without Ac<sub>4</sub>ManAz, and subsequently purified using ultrafiltration (4347 × g, 40 min) and a qEV column. The purified EVs were lysed and assessed for protein content using a BCA assay kit (Sigma, USA). Laemmli sample buffer was added to the lysates, followed by boiling at 100 °C for 5 min. Subsequently, 10  $\mu g$  of proteins were loaded and electrophoresed on a 12% acrylamide gel (Tris-Glycine/SDS running buffer). The protein bands were then transferred to a PVDF membrane (transfer buffer: 25 mM Tris base, 190 mM glycine, and 20% methanol), and the membrane was stained with an HRP-conjugated OVA polyclonal antibody. EVs derived from B16-F10 cells served as the negative control. EVs were also stained with anti-Tsg101 and anti-CD63 and HRP-conjugated secondary antibody, and visualized using chemiluminescence.

# **Endocytosis of EVs by DCs**

DCs were seeded on the coverslips at a density of  $6 \times 10^5$  cells and allowed to attach overnight. Cells were incubated with EV-Cy5 for

30 mins or 4 h and washed with PBS. Cells were stained with Rab5 antibody at a dilution of 1:50 and FITC-conjugated Goat anti-rabbit IGG (H+L) or Alexa Fluor 488 conjugated LAMP-1 monoclonal antibody at 1:100 in 0.1% BSA and incubated at 4 °C followed by washing with PBS and fixing the cells with 4% paraformaldehyde solution. Nuclei were stained with DAPI at 1:5000 dilution followed by multiple washes with PBS. The coverslips were mounted onto microscopic slides and imaged using a confocal laser scanning microscope.

#### **ELISA** assay

96-well high binding ELISA plates were coated with 200  $\mu$ L of pure OVA protein (0.1 ng/mL to 100 ng/mL) and EV samples (serial dilution from 1/2, 1/10 to 1/10000) in coating buffer (3 replicates each) for overnight at 4 °C. The plate was washed with PBST three times followed by the addition of the blocking buffer (5% non-fat milk in PBST) to each well and incubated for 2 h at room temperature in a shaking platform. The plate was washed with PBST 3 times. 50  $\mu$ L of horseradish peroxidase (HRP) conjugated ovalbumin polyclonal antibody (1:5000) in blocking buffer was added to each well and incubated at room temperature for 2 h. 100  $\mu$ L of substrate was added to each well, allowing the color to change for 15 min. Finally, 50  $\mu$ L of stop solution (2 M sulfuric acid) was added to terminate the enzymatic reaction. The optical density was measured at a wavelength of 405 nm using a plate reader.

#### Immune cell analysis in fibrotic tissue

EV/CpG gels ( $7 \times 10^8$  EVs and 12.72 ng of CpG) or EV gels ( $7 \times 10^8$  EVs) were subcutaneously injected to C57BL/6 mice on day 0. On day 3 or day 7, the fibrotic capsule surrounding the gels was harvested for immune cell analysis. Fibrotic tissues were disrupted, digested, and passed through cell strainers, stained with fluorophore-conjugated antibodies, and analyzed using a flow cytometer.

#### Anti-OVA IgG titer detection

C57BL/6 mice were subcutaneously injected with EV/CpG gel  $(7 \times 10^8)$  EVs and 12.72 ng of CpG), EV gel  $(7 \times 10^8 \text{ EVs})$ , the mixture of EV  $(7 \times 10^8 \text{ EVs})$ , DBCO-PEG, and CpG (12.72 ng), or PBS on day 0. Blood samples were collected on day 5, 7, 12, and 18 respectively. Blood was centrifuged at  $2000 \times g$  for 5 min to collect the serum, which was stored at -80 °C until further use. For the detection of anti-OVA IgG titers, 96-well high-binding ELISA plates were coated overnight at 4 °C with OVA (20 μg/mL, 50 μL per well) and were further blocked with the blocking buffer for 2 h at room temperature in on shaking platform. After 2-3 washing steps with PBST, diluted serum samples (1/10, 1/100, 1/1000, 1/10000, 1/100000) were added to triplicate wells. The plates were then incubated at room temperature for 2 h followed by washing with PBST 10 times. Biotinylated goat anti-mouse-IgG secondary antibody (1:500) in blocking buffer was added to each well and incubated at room temperature for 2 h. After washing with PBST 8 times, HRP-streptavidin (1:500) in PBST was added to each well and incubated for 1h at room temperature. Peroxidase activity was determined by adding 100 µL of the substrate solution to each well for 30 min. Finally, 50 µL of stop solution (2 M sulfuric acid) was added to terminate the enzymatic reaction. The color was quantified by using a plate reader at 405 nm. The anti-OVA IgG titer was determined by serum dilution.

#### **Blood test**

C57BL/6 mice were subcutaneously injected with an EV/CpG gel (containing  $7 \times 10^8$  EVs and 12.72 ng of CpG) or an EV gel (containing  $7 \times 10^8$  EVs) on day 0. Blood samples were collected via the retro-orbital method at days 3, 6, and 9 post-injection of EV gels. White blood cell (WBC), red blood cell (RBC), lymphocyte, monocyte, and granulocyte counts were assessed by staining the cells with anti-TER119, anti-CD45, anti-CD3, anti-CD15, anti-CD19, anti-CD14, anti-CD41, and anti-Ly6C, followed by flow cytometry analysis.

#### Cytokine analysis

The levels of inflammatory cytokines at the injection sites of EV gel or EV/CpG gel were assessed using a proteome profiling assay (Proteome Profiler Mouse Cytokine Array Kit, Panel A). In brief, C57BL/6 mice received subcutaneous injections of either an EV/CpG gel (containing  $7 \times 10^8$  EVs and 12.72 ng CpG) or an EV gel (containing  $7 \times 10^8$  EVs). Three days after the injection, the supernatant of cells collected near the gel injection site was processed for cytokine analysis. To prepare the samples, the collected medium was centrifuged to eliminate dead cells and debris. Reagents were prepared in accordance with the manufacturer's instructions (R&D, USA). The membranes were initially blocked by incubating with Array Buffer 6 for 1h on a shaker. Each sample was diluted by adding 1 mL of the collected medium to 0.5 mL of Array Buffer 4, and the volume was adjusted to 1.5 mL with Array Buffer 6. Then, 15 µL of the mouse cytokine detection antibody cocktail was added to each sample and incubated for 1h. Following the incubation, the membranes were washed and incubated with the antibody-sample mixture overnight at 4 °C. On the following day, the membranes were washed again and incubated with Streptavidin-HRP (1:2000) for 30 min at room temperature. After a final wash, 1 mL of Chemi Reagent mix was applied to each membrane, which was then exposed to a chemiluminescence imager for 2-5 min. Positive signals on the membranes were identified using a transparency overlay template provided by the manufacturer, aligning it with the reference spots for each cytokine. Pixel densities (average signals from duplicate spots) were analyzed using ImageJ software, with background signal subtracted from the average signal.

#### Vaccination and prophylactic study

C57BL/6 mice were divided into five groups: EV/CpG gel  $(7 \times 10^8 \text{ EVs})$ and 12.72 ng of CpG), EV gel + CpG (7 × 10<sup>8</sup> EVs and 12.72 ng of CpG), OVA (50  $\mu$ g) and CpG (50  $\mu$ g), EV gel (7 × 10<sup>8</sup> EVs), or PBS. EV gels or the solution of OVA and CpG or PBS were subcutaneously injected into the flank of mice on day 0. Blood was drawn on days 6, 9, and 14 for the analysis of SIINFEKL-specific CD8<sup>+</sup> T cells in PBMCs<sup>62</sup>. For tetramer analysis. PBMCs were stained with fluorophore-conjugated SIINFEKL tetramer, anti-CD3, anti-CD8, and e780 fixable viability dye for 20 min, and analyzed on a flow cytometer. For IFN-y restimulation, PBMCs were treated with SIINFEKL peptide for 1.5 h and Golgi plug for 2.5 h, and then stained with fluorophore-conjugated anti-CD3, anti-CD8, and e780 fixable viability dye. Cells were further treated with the fixation & permeabilization buffer and stained with fluorophore-conjugated anti-IFN-γ for flow cytometry analysis<sup>62</sup>. On day 15, E.G7-OVA tumor cells (100k cells in 50 μL of HBSS) were subcutaneously injected into C57BL/ 6 mice. The tumor volume and body weight of the mice were measured twice a week. Tumor volume was calculated using the formula  $L \times W^2/2$ (L = long axis diameter; W = short axis diameter). The endpoint was defined as the day the largest diameter of tumors reaches 20 mm, or animals become moribund, or animals have a body weight loss of >20%, or animals have a body condition of 2 or less on a 5 point scale.

# Therapeutic tumor study of EV hydrogel vaccines

E.G7-OVA cells (500k cells in 50 µL of HBSS) were subcutaneously injected into the right flank of C57BL/6 mice on day 0. When the tumors reached a diameter of 5–7 mm, the mice were randomly divided into five groups: EV/CpG gel +  $\alpha$ -PD-1, EV/CpG gel, EV gel,  $\alpha$ -PD-1, or PBS. Gels were injected on day 9.  $\alpha$ -PD-1 (100 µg per dose) was intraperitoneally injected on days 13, 16, and 19. The tumor volume and mouse body weight were measured 2-3 times a week. Tumor volume was calculated using the formula L  $\times$  W²/2 (L = long axis diameter; W = short axis diameter)  $^{62}$ . The endpoint was defined as the day the largest diameter of tumors reaches 20 mm, or animals become moribund, or animals have a body weight loss of >20%, or animals have a body condition of 2 or less on a 5 point scale.

#### **Tumor microenvironment analysis**

C57BL/6 mice were assigned to seven experimental groups: EV/CpG gel ( $7 \times 10^8$  EVs and 12.72 ng CpG), EV gel + CpG ( $7 \times 10^8$  EVs and 12.72 ng CpG), OVA ( $50 \mu g$ ) and CpG (50 ng), EV gel ( $7 \times 10^8$  EVs), EV only ( $7 \times 10^8$  EVs), unconjugated EV + DBCO-PEG + CpG ( $7 \times 10^8$  EVs and 12.72 ng CpG), or PBS. On Day 0, E.G7-OVA cells (200,000) were washed with HBSS buffer and subcutaneously injected into the upper right flank of the mice. On Day 12, the respective EV gel formulations were injected subcutaneously. Tumors and gels were harvested on Day 15 for further analysis. For processing, tumors and gels were mechanically disrupted using a syringe plunger, then passed through a 40  $\mu$ m cell strainer and rinsed with 10 mL of RPMI. The resulting cell suspension was collected, washed with PBS, and stained for flow cytometry analysis.

#### Statistical analysis

For comparisons between two groups, we used two-tailed Welch's t test or two-tailed Student's t test. For multiple comparisons, we used one-way analysis of variance (ANOVA) with a post hoc Fisher's LSD test. The results were deemed significant at  $0.01 < P \le 0.05$ , highly significant at  $0.001 < P \le 0.01$ , and extremely significant at  $0.001 < P \le 0.001$ .

#### **Reporting summary**

Further information on research design is available in the Nature Portfolio Reporting Summary linked to this article.

# **Data availability**

Source data for all figures have been provided and will be published alongside this paper. All data underlying this study are available from the corresponding author upon request. Source data are provided with this paper.

#### References

- Kang, T., Atukorala, I. & Mathivanan, S. Biogenesis of Extracellular Vesicles. Subcell. Biochem 97, 19–43 (2021).
- Herrmann, I. K., Wood, M. J. A. & Fuhrmann, G. Extracellular vesicles as a next-generation drug delivery platform. *Nat. Nanotechnol.* 16, 748–759 (2021).
- Gurung, S., Perocheau, D., Touramanidou, L. & Baruteau, J. The exosome journey: from biogenesis to uptake and intracellular signalling. Cell Commun. Signal 19, 47–47 (2021).
- Kalluri, R. & LeBleu, V. S. The biology, function, and biomedical applications of exosomes. Science 367, eaau6977 (2020).
- Tenchov, R. et al. Exosomes—Nature's Lipid Nanoparticles, a Rising Star in Drug Delivery and Diagnostics. ACS Nano 16, 17802–17846 (2022).
- Shao, J., Zaro, J. & Shen, Y. Advances in Exosome-Based Drug Delivery and Tumor Targeting: From Tissue Distribution to Intracellular Fate. *Int. J. Nanomed.* 15, 9355–9371 (2020).
- György, B., Hung, M. E., Breakefield, X. O. & Leonard, J. N. Therapeutic applications of extracellular vesicles: clinical promise and open questions. *Annu. Rev. Pharm. Toxicol.* 55, 439–464 (2015).
- Wiklander, O. P. B., Brennan, M., Lötvall, J., Breakefield, X. O. & El Andaloussi, S. Advances in therapeutic applications of extracellular vesicles. Sci. Transl. Med. 11, aav8521 (2019).
- Skog, J. et al. Glioblastoma microvesicles transport RNA and proteins that promote tumour growth and provide diagnostic biomarkers. Nat. Cell Biol. 10, 1470–1476 (2008).
- Vader, P., Breakefield, X. O. & Wood, M. J. Extracellular vesicles: emerging targets for cancer therapy. *Trends Mol. Med.* 20, 385–393 (2014).
- D'Souza-Schorey, C. & Clancy, J. W. Tumor-derived microvesicles: shedding light on novel microenvironment modulators and prospective cancer biomarkers. Genes Dev. 26, 1287–1299 (2012).

- Li, Y. et al. Exosomes as promising bioactive materials in the treatment of spinal cord injury. Stem Cell Res. Ther. 15, 335 (2024).
- Lai, R. C., Chen, T. S. & Lim, S. K. Mesenchymal stem cell exosome: a novel stem cell-based therapy for cardiovascular disease. *Regen. Med.* 6, 481–492 (2011).
- Timmers, L. et al. Human mesenchymal stem cell-conditioned medium improves cardiac function following myocardial infarction. Stem Cell Res. 6, 206–214 (2011).
- Wang, C. et al. Macrophage-Derived mir-155-Containing Exosomes Suppress Fibroblast Proliferation and Promote Fibroblast Inflammation during Cardiac Injury. Mol. Ther. 25, 192–204 (2017).
- He, S. et al. Endothelial extracellular vesicles modulate the macrophage phenotype: Potential implications in atherosclerosis. Scand. J. Immunol. 87, e12648 (2018).
- Hofmann, U. et al. Activation of CD4+ T lymphocytes improves wound healing and survival after experimental myocardial infarction in mice. Circulation 125, 1652–1663 (2012).
- Weirather, J. et al. Foxp3+ CD4+ T cells improve healing after myocardial infarction by modulating monocyte/macrophage differentiation. Circ. Res. 115, 55–67 (2014).
- Manzoor, T. et al. Extracellular vesicles derived from mesenchymal stem cells — a novel therapeutic tool in infectious diseases. *Inflamm. Regen.* 43, 17 (2023).
- Kou, M. et al. Mesenchymal stem cell-derived extracellular vesicles for immunomodulation and regeneration: a next generation therapeutic tool? Cell Death Dis. 13, 580 (2022).
- Nassar, W. et al. Umbilical cord mesenchymal stem cells derived extracellular vesicles can safely ameliorate the progression of chronic kidney diseases. *Biomater. Res.* 20, 21 (2016).
- Kabat, M., Bobkov, I., Kumar, S. & Grumet, M. Trends in mesenchymal stem cell clinical trials 2004-2018: Is efficacy optimal in a narrow dose range? Stem Cells Transl. Med. 9, 17–27 (2020).
- Duong, A., Parmar, G., Kirkham, A. M., Burger, D. & Allan, D. S. Registered clinical trials investigating treatment with cell-derived extracellular vesicles: a scoping review. Cytotherapy 25, 939–945 (2023).
- Zhang, T. et al. CRISPR-Cas12a powered hybrid nanoparticle for extracellular vesicle aggregation and in-situ microRNA detection. Biosens. Bioelectron. 245, 115856 (2024).
- Zhang, M. et al. Engineered exosomes from different sources for cancer-targeted therapy. Sig. Transduct. Target Ther. 8, 124 (2023).
- Yang, Q. et al. Exosome-based delivery strategies for tumor therapy: an update on modification, loading, and clinical application. J. Nanobiotechnol. 22, 41 (2024).
- Xue, X. et al. An exosomal strategy for targeting cancer-associated fibroblasts mediated tumors desmoplastic microenvironments. J. Nanobiotechnol. 22, 196 (2024).
- Qin, C. et al. The systematic role of pancreatic cancer exosomes: distant communication, liquid biopsy and future therapy. Cancer Cell Int. 24, 264 (2024).
- Kamerkar, S. et al. Exosome-mediated genetic reprogramming of tumor-associated macrophages by exoASO-STAT6 leads to potent monotherapy antitumor activity. Sci. Adv. 8, eabj7002 (2022).
- 30. Johnson, J. et al. First-in-human clinical trial of allogeneic, platelet-derived extracellular vesicles as a potential therapeutic for delayed wound healing. *J. Extracell. Vesicles* **12**, e12332 (2023).
- 31. Dionisi, M. et al. Tumor-Derived Microvesicles Enhance Cross-Processing Ability of Clinical Grade Dendritic Cells. *Front. Immunol.* **9**, 2481 (2018).
- Rughetti, A. et al. Microvesicle cargo of tumor-associated MUC1 to dendritic cells allows cross-presentation and specific carbohydrate processing. Cancer Immunol. Res. 2, 177–186 (2014).
- Zhang, H. et al. Cell-free tumor microparticle vaccines stimulate dendritic cells via cGAS/STING signaling. Cancer Immunol. Res. 3, 196–205 (2015).

- Luo, R. et al. Emerging Diagnostic Potential of Tumor-derived Exosomes. J. Cancer 12, 5035–5045 (2021).
- Xu, Z., Zeng, S., Gong, Z. & Yan, Y. Exosome-based immunotherapy: a promising approach for cancer treatment. *Mol. Cancer* 19, 160 (2020).
- Morishita, M., Takahashi, Y., Matsumoto, A., Nishikawa, M. & Takakura, Y. Exosome-based tumor antigens-adjuvant co-delivery utilizing genetically engineered tumor cell-derived exosomes with immunostimulatory CpG DNA. *Biomaterials* 111, 55–65 (2016).
- Rezaie, J., Feghhi, M. & Etemadi, T. A review on exosomes application in clinical trials: perspective, questions, and challenges. *Cell Commun. Signal.* 20, 145 (2022).
- 38. Escudier, B. et al. Vaccination of metastatic melanoma patients with autologous dendritic cell derived-exosomes: results of thefirst phase I clinical trial. *J. Transl. Med.* **3**, 10 (2005).
- 39. Dai, S. et al. Phase I clinical trial of autologous ascites-derived exosomes combined with GM-CSF for colorectal cancer. *Mol. Ther.* **16**, 782–790 (2008).
- Lee, B. C., Kang, I. & Yu, K. R. Therapeutic Features and Updated Clinical Trials of Mesenchymal Stem Cell (MSC)-Derived Exosomes. J. Clin. Med. 10, 711 (2021).
- 41. Liang, X., Ding, Y., Zhang, Y., Tse, H.-F. & Lian, Q. Paracrine Mechanisms of Mesenchymal Stem Cell-Based Therapy: Current Status and Perspectives. *Cell Transplant.* **23**, 1045–1059 (2014).
- Jafarinia, M., Alsahebfosoul, F., Salehi, H., Eskandari, N. & Ganjalikhani-Hakemi, M. Mesenchymal Stem Cell-Derived Extracellular Vesicles: A Novel Cell-Free Therapy. *Immunological Investig.* 49, 758–780 (2020).
- Shi, M. M. et al. Preclinical efficacy and clinical safety of clinical-grade nebulized allogenic adipose mesenchymal stromal cells-derived extracellular vesicles. J. Extracell. Vesicles 10, e12134 (2021).
- Zhang, B., Sim, W. K., Shen, T. L. & Lim, S. K. Engineered EVs with pathogen proteins: promising vaccine alternatives to LNP-mRNA vaccines. J. Biomed. Sci. 31, 9 (2024).
- Zhou, Q. et al. Tumor-derived extracellular vesicles in melanoma immune response and immunotherapy. *Biomed. Pharmacother*. 156, 113790 (2022).
- Xiao, L., Erb, U., Zhao, K., Hackert, T. & Zöller, M. Efficacy of vaccination with tumor-exosome loaded dendritic cells combined with cytotoxic drug treatment in pancreatic cancer. *Oncoimmunology* 6, e1319044 (2017).
- Choo, Y. W. et al. M1 Macrophage-Derived Nanovesicles Potentiate the Anticancer Efficacy of Immune Checkpoint Inhibitors. ACS Nano 12, 8977–8993 (2018).
- Willekens, F. L. et al. Liver Kupffer cells rapidly remove red blood cell-derived vesicles from the circulation by scavenger receptors. *Blood* 105, 2141–2145 (2005).
- 49. Xie, Y. et al. Hydrogels for Exosome Delivery in Biomedical Applications. Gels **8**, 328 (2022).
- Tang, J. et al. A DNA-based hydrogel for exosome separation and biomedical applications. *Proc. Natl Acad. Sci.* 120, e2303822120 (2023).
- 51. Fan, L. et al. Exosomes-loaded Electroconductive hydrogel synergistically promotes tissue repair after spinal cord injury via Immunoregulation and enhancement of myelinated axon growth. *Adv. Sci.* **9**, 2105586 (2022).
- 52. Tang, J. et al. Injection-free delivery of MSC-derived extracellular vesicles for myocardial infarction therapeutics. *Adv. Healthc. Mater.* **11**, 2100312 (2022).
- 53. Bhatta, R. et al. Metabolic tagging of extracellular vesicles and development of enhanced extracellular vesicle based cancer vaccines. *Nat. Commun.* **14**, 8047 (2023).
- Ju, Y., Hu, Y., Yang, P., Xie, X. & Fang, B. Extracellular vesicle-loaded hydrogels for tissue repair and regeneration. *Mater. Today Bio* 18, 100522 (2023).

- Huang, J. et al. Cell-free exosome-laden scaffolds for tissue repair.
  Nanoscale 13. 8740–8750 (2021).
- Laughlin, S. T., Baskin, J. M., Amacher, S. L. & Bertozzi, C. R. In Vivo Imaging of Membrane-Associated Glycans in Developing Zebrafish. Science 320, 664–667 (2008).
- 57. Laughlin, S. T. & Bertozzi, C. R. Metabolic labeling of glycans with azido sugars and subsequent glycan-profiling and visualization via Staudinger ligation. *Nat. Protoc.* **2**, 2930 (2007).
- 58. Wang, H. & Mooney, D. J. Metabolic glycan labelling for cancer-targeted therapy. *Nat. Chem.* **12**, 1102–1114 (2020).
- Wang, H. et al. Selective in vivo metabolic cell-labeling-mediated cancer targeting. Nat. Chem. Biol. 13, 415 (2017).
- Wang, H. et al. Metabolic labeling and targeted modulation of dendritic cells. Nat. Mater. 19, 1244–1252 (2020).
- Wang, H. et al. Targeted Ultrasound-Assisted Cancer-Selective Chemical Labeling and Subsequent Cancer Imaging using Click Chemistry. Angew. Chem. Int. Ed. 55, 5452–5456 (2016).
- Han, J. et al. Metabolic glycan labeling immobilizes dendritic cell membrane and enhances antitumor efficacy of dendritic cell vaccine. Nat. Commun. 14, 5049 (2023).
- 63. Xie, R. et al. In vivo metabolic labeling of sialoglycans in the mouse brain by using a liposome-assisted bioorthogonal reporter strategy. *Proc. Natl Acad. Sci.* **113**, 5173–5178 (2016).

# **Acknowledgements**

The authors would like to acknowledge the financial support from NSF DMR 2143673 CAR (H.W.), NIH R01CA274738 (H.W.), NIH R21CA270872 (H.W.), Sontag Foundation Distinguished Scientist Award (H.W.), and American Cancer Society Research Scholar Grant RSG-24-1318096-01-RMC (H.W.). This material is based upon work supported by the Air Force Office of Scientific Research under award number FA9550-23-1-0609 (Q.C. and H.W.). Research reported in this publication was supported by the Cancer Scholars for Translational and Applied Research (C\*STAR) Program sponsored by the Cancer Center at Illinois and the Carle Cancer Center under Award Number CST EP012023.

# **Author contributions**

R.B. and H.W. designed the study and led the analysis and writing of the manuscript. R.B., J.H., Y.L., Y.B., Y.W., and D.N. performed the experiments. R.B., J.H., Y.L., Y.B., Y.W., D.N., Q.C., and H.W. contributed to data analysis and manuscript revision.

# **Competing interests**

H.W. and R.B. filed a patent application for the extracellular vesicle hydrogel technology. Other authors declare no competing interests.

# **Additional information**

**Supplementary information** The online version contains supplementary material available at https://doi.org/10.1038/s41467-025-59278-0.

**Correspondence** and requests for materials should be addressed to Hua Wang.

**Peer review information** *Nature Communications* thanks Gregor Fuhrmann, Alireza Hassani Najafabadi and Magdalena J. Lorenowicz for their contribution to the peer review of this work. A peer review file is available.

**Reprints and permissions information** is available at http://www.nature.com/reprints

**Publisher's note** Springer Nature remains neutral with regard to jurisdictional claims in published maps and institutional affiliations.

Open Access This article is licensed under a Creative Commons Attribution-NonCommercial-NoDerivatives 4.0 International License, which permits any non-commercial use, sharing, distribution and reproduction in any medium or format, as long as you give appropriate credit to the original author(s) and the source, provide a link to the Creative Commons licence, and indicate if you modified the licensed material. You do not have permission under this licence to share adapted material derived from this article or parts of it. The images or other third party material in this article are included in the article's Creative Commons licence, unless indicated otherwise in a credit line to the material. If material is not included in the article's Creative Commons licence and your intended use is not permitted by statutory regulation or exceeds the permitted use, you will need to obtain permission directly from the copyright holder. To view a copy of this licence, visit http://creativecommons.org/licenses/by-nc-nd/4.0/.

© The Author(s) 2025